https://doi.org/10.5194/nhess-2024-109
Preprint. Discussion started: 19 July 2024

Natural Hazards and Earth System Sciences
Discussions

Optimizing Rainfall-Triggered Landslide Thresholds to Warning Daily Landslide Hazard in Three Gorges Reservoir Area

Bo Peng[1], Xueling Wu[1]

[1]School of Geophysics and Geomatics, China University of Geosciences, Wuhan 430074, China

Correspondence to: Xueling Wu (wuxl@cug.edu.cn)

Abstract. Rainfall is intrinsically connected to the incidence of landslide catastrophes. Exploring the ideal rainfall threshold model (RTM) for an area in order to determine the rainfall warning level (RWL) for the region for daily landslide hazard warning (LHW) is critical for precise prevention and management of local landslides. In this paper, a method for calculating rainfall thresholds using multilayer perceptron (MLP) regression is proposed for 453 rainfall-induced landslides. First, the study area was divided into subareas based on topography and climate conditions. Then, two methods, MLP and ordinary least squares (OLS), were utilized to explore the optimal RTM for each subregion. Subsequently, 11 factors along with three models were selected to predict landslide susceptibility (LS). Finally, to obtain daily LHW result for the study area, a superposition matrix was employed to overlay the daily RWL with the ideal LS prediction results. The following are the study's findings: (1) The optimal RTMs and calculation methods are different for different subregions. (2) The Three-dimensional convolutional neural network model produces more accurate LS prediction results. (3) The daily LHW was validated using anticipated rainfall data for July 19, 2020, and the validation results proved the correctness of the LHW results and RTM.

1 Introduction

Landslide catastrophes accounted for 71.55% of geological disasters in China from 2005 to 2021, according to the China Statistical Yearbook (http://www.stats.gov.cn/sj/ndsj/). Frequent landslide catastrophes endanger people's lives and property (Xing et al., 2021). Rainfall will lead to landslide disasters by changing the pore pressure in the soil body (Zhao et al., 2022) and weakening the shear strength of the geotechnical body (Chan et al., 2018). According to research (Marin et al., 2020; Yuniawan et al., 2022): rainfall is intrinsically connected to the great majority of landslide deformation and instability. Therefore, it is significant to delineate the rainfall thresholds for different rainfall conditions and areas through the study for the fine development of landslide hazard warning (LHW) and disaster prevention and control. LHW is described as the conditional prediction of probable landslide temporal and spatial probability under the limitations of triggering and inducing variables (Budimir et al., 2015). The rainfall warning level (RWL) (i.e., the temporal probability of landslide occurrence) calculated by the rainfall threshold model (RTM) is the triggering factor in this study, and the inducing factor is the

https://doi.org/10.5194/nhess-2024-109
Preprint. Discussion started: 19 July 2024


Natural Hazards and Earth System Sciences Discussions

prediction result of landslide susceptibility (LS) (i.e., the spatial probability of landslide occurrence) calculated by the susceptibility model.

The spatial probability of landslide occurrence can be reflected by LS (Huang et al., 2022b). General linear models (Aksha et al., 2020), information value models (Yu et al., 2022), machine learning models, and others are among the methods used to predict LS. Machine learning models can fit and predict the nonlinear relationship between LS and landslide predisposing factors more effectively than other kinds of models (Guo et al., 2021). Commonly used machine learning models include logistic regression (Baharvand et al., 2020), artificial neural networks (Jiang et al., 2014), support vector machines (SVM) (Zhu and Hu, 2012), random forests (RF) (Chen et al., 2014), Bayesian algorithms (He et al., 2019) and deep learning algorithms (Huang et al., 2020). However, determining which model is best suited for LS prediction is challenging, and there is great uncertainty in the LS prediction results of various machine learning models (Xia et al., 2020). Even little improvements in LS prediction accuracy might have a significant influence on LS zoning (Chen et al., 2018). Therefore, to decrease the uncertainty of LS results, different susceptibility models are frequently employed to predict LS in the study area, and the model with the greatest accuracy is chosen.

RTM approaches primarily include of deterministic methods based on physical and hydrological models, as well as empirical methods based on landslide cataloguing and rainfall event statistics (Chung et al., 2017; Wu et al., 2015). The former establishes the relationship between rainfall and landslide stability through dynamic hydrological models and determines the critical rainfall threshold for landslide instability in the physical model (Ciurleo et al., 2019). However, due to the difficulty in accurately obtaining hydrological parameters and geotechnical parameters on a large scale, this method is only applicable to smaller study area (Wu and Yeh, 2020). The latter is mainly derived by calculating the relationship between historical landslide and rainfall data (Abraham et al., 2020a; Pradhan et al., 2019). This method is widely used because of its advantages of convenience in data acquisition, strong applicability, and excellent results (Martinovic et al., 2018). Currently, commonly used RTM include the intensity of rainfall - duration of rainfall (I-D) threshold model (Abraham et al., 2019; Lee et al., 2014) and effective rainfall - duration of rainfall (E-D) threshold model (Abraham et al., 2020b; Peruccacci et al., 2017). The regression methods used to calculate the RTM include logistic regression (Mathew et al., 2014), ordinary least squares (OLS) regression (Rossi et al., 2017) and quantile regression (Salee et al., 2022). There are differences in the applicability of different RTM and different regression methods in different regions (Marin, 2020; Segoni et al., 2018). Therefore, to decrease uncertainty in LHW, several regression methods and RTM must be used to establish the best appropriate rainfall threshold for a certain location.

Given that many researchers have employed the log-log coordinates system for RTM regression analysis (He et al., 2020), this study proposes to use MLP regression method to study the rainfall thresholds under various rainfall durations. Simultaneously, the third dimension indicator "rainfall for the day" (R) was introduced to create the E-D-R RTM based on the E-D RTM (Liu et al., 2022).

https://doi.org/10.5194/nhess-2024-109
Preprint. Discussion started: 19 July 2024


Natural Hazards and Earth System Sciences
Discussions

In this study, the Three Gorges Reservoir Area (TGRA) was used as the study area, and the landslides were first catalogued to get the E and D data during the five days before the landslides, as well as the R data at the time of the landslides. Following that, the rainfall thresholds corresponding to the E-D and E-D-R models for distinct landslide occurrence probabilities were calculated using both OLS and MLP regression methods, respectively. To explore the optimal RTM for the study area and the feasibility of neural network for RTM research, as well as to categorize RWL based on the optimal RTM. Then, select the factors that induce landslide occurrence and predict the LS results using RF, SVM, and 3D convolutional neural network (CNN-3D) models, and utilize the LS results with the best accuracy as the spatial probability of landslide occurrence in the study area. Finally, the daily RWL is combined with the LS result using the superposition matrix to achieve the daily LHW, which serves as a reference for precision prevention and management of local landslide disasters.

2. Methods

2.1 Rainfall Threshold Model

2.1.1 OLS Regression

OLS regression is a commonly used linear regression method that can be used to establish a linear relationship between the independent variable (x) and the dependent variable (y). It minimizes the error between the predicted value and the actual observed value by seeking the slope and intercept that best fits the data (Lim et al., 2023).

The basic form of its regression model can be expressed as:

$$y = \beta_0 + \sum_{i=1}^{n} \beta_i x_i \,, \tag{1}$$

where y denotes the dependent variable, x_i denotes the independent variable, n denotes the number of independent variables, β_i denotes the coefficients of the independent variables, and β_0 denotes the constant intercept.

2.1.2 MLP Regression

MLP is a common neural network with the ability of nonlinear mapping, which can learn complex nonlinear functional relationships through multiple layers of nodes. Currently, it has been widely used in many fields such as geospatial analysis (Hasan et al., 2023; Wang et al., 2023b), aerodynamics (Barcenas et al., 2023), atmospheric science (Hoffman and Jasinski, 2023), rainfall prediction (Narimani et al., 2023), and image fusion (Mei et al., 2023). In the regression analysis of scatter data, a scatter data set can be regarded as composed of multiple input-output data pairs, and the model adjusts the weights of the model by minimizing the error between the predicted value and the actual data, and finally realizes the regression of scatter data. In this study, we built an MLP model with two hidden layers (Fig. 1).

https://doi.org/10.5194/nhess-2024-109
Preprint. Discussion started: 19 July 2024

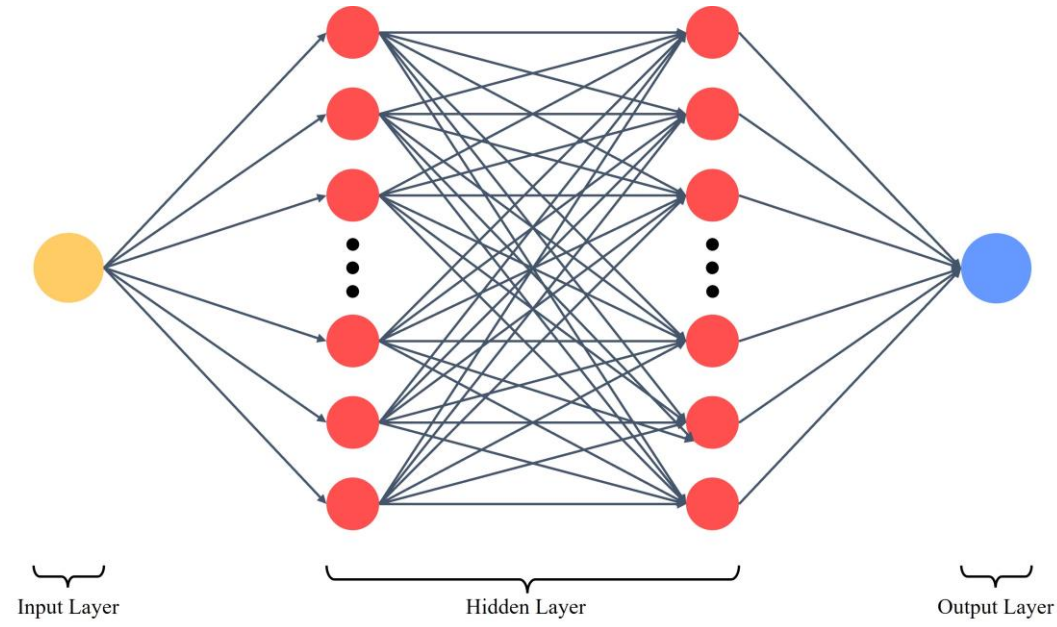

Figure 1: Schematic diagram of the MLP model.

2.1.3 E-D-R Rainfall Threshold Model

The E-D-R RTM is based on the E-D RTM, with the introduction of the R metrics at the third latitude to optimize the original RTM. To investigate the E-D-R RTM, the E-D RTM must first be determined.

The E-D RTM aims to investigate the effective rainfall as a function of duration of rainfall (Teja et al., 2019). The scatter is generally analyzed by regression in a log-log coordinates system, and then the resulting fitted straight line is transformed into a result in a Cartesian coordinate system. The expression for this is:

$$E = \alpha \times D^{\beta} , \quad (2)$$

Assume that the linear equation obtained by fitting in the log-log coordinates system has an intercept of b and a slope of a. Then, in the above equation, $\alpha = 10^{b}$, $\beta = a$, and D denotes the duration of rainfall (d). E is the effective rainfall (mm), which refers to the total amount of rainfall that actually infiltrates and acts on the landslide body in addition to the slope runoff and evaporation (Huang et al., 2022a). The effective rainfall formula used in this study is as follows:

$$E = \sum_{i=1}^{n} k^{i-1} E_i , \quad (3)$$

where E denotes the effective rainfall, E_i is the rainfall on the previous i days, and k is the effective rainfall coefficient. The value of k is usually set to 0.8 (Huang et al., 2022a). Furthermore, it has been shown that the effective rainfall in the first 5 days of the TGRA has a strong link with landslide events (Zhou et al., 2022). Therefore, the number of days of rainfall statistics n in this work is set to 5.

https://doi.org/10.5194/nhess-2024-109
Preprint. Discussion started: 19 July 2024

Natural Hazards and Earth System Sciences
Discussions

The third dimension of the indicator R is added based on the E-D RTM to expand the threshold model from two to three dimensions, and the RTL meet the following relational equation:

$$T = \max\{G_E, G_R\}\,, \tag{4}$$

where T denotes the final RWL, while G_E and G_R denote the RWL for the E-D model and R, respectively.

2.2 CNN-3D Model

Convolutional Neural Network (CNN) is a deep learning algorithm, widely used in image recognition (Fan et al., 2022; Gill et al., 2022), natural language processing (Jin et al., 2023; Kaliyar et al., 2021) and other domains. Its primary concept is to extract features from input data using a convolution operation (Youssef et al., 2022). However, for one- and two-dimensional CNNs, feature extraction for induced factor data is only performed at a single raster point. Both methods ignore the spatial information around the raster points (Yang et al., 2022). As a result, this study presents CNN-3D in order to fully use the rich spatial information around the raster points in order to increase the prediction accuracy of LS. The structure of CNN-3D is similar to that of CNN, but since the input data contains more information, CNN-3D can provide more accurate results (Liu et al., 2023).

We picked a three-dimensional structure to create samples in this experiment. Before producing the samples, an n-channel picture is formed by superimposing n components. Each pixel is then extended outwards by 7 pixels to generate a 15 × 15 × n image as input. Subsequently, through operations such as convolution and pooling in the hidden layer, the high-level features are mapped to the low-dimensional space and stored in the neural units of the fully connected layer, and finally classified using the Softmax function to obtain the results of landslides and non-slides (Fig. 2).

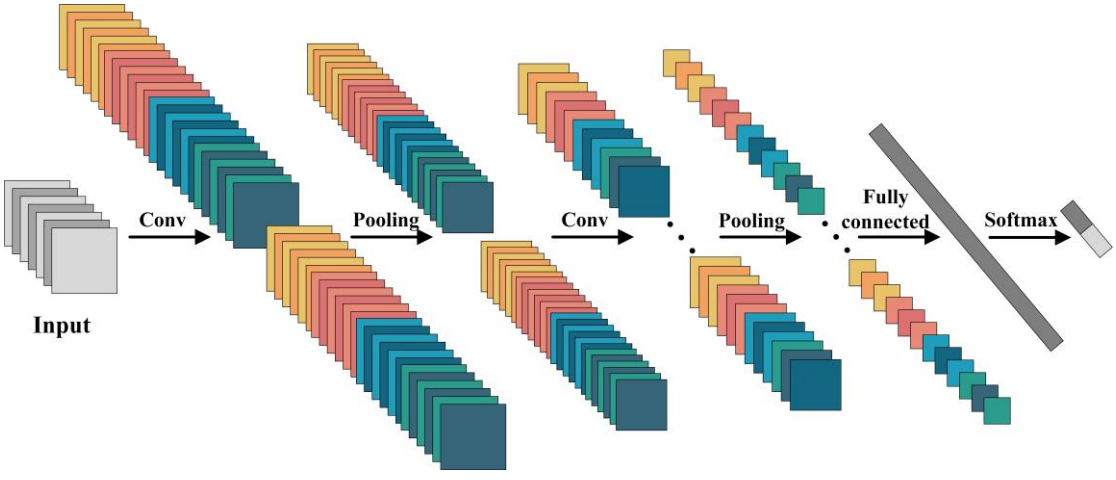

Figure 2: Schematic diagram of CNN-3D structure.

https://doi.org/10.5194/nhess-2024-109
Preprint. Discussion started: 19 July 2024

Natural Hazards and Earth System Sciences
Discussions

3. Overview of the Study Area

3.1 Physical and Geographical Characteristics

The study area is located in the upper reaches of the Yangtze River between Sandouping in Yichang City and Jiangjin District in Chongqing, which is situated at longitude 105°50′- 111°42′ E and latitude 28°30′-31°45′ N (Cheng et al., 2022), encompassing a total of 29 administrative districts and counties in Hubei Province and Chongqing Municipality (7 districts and counties in Hubei, and 22 districts and counties in Chongqing), and covering a total area of $5.67\times10^4 km^2$ (Fig. 3).The climate of the region is subtropical monsoon with an average annual precipitation of 445-1813 mm (Long et al., 2021). And the abundant rainfall in the area is a major factor inducing landslides (Guo et al., 2022).

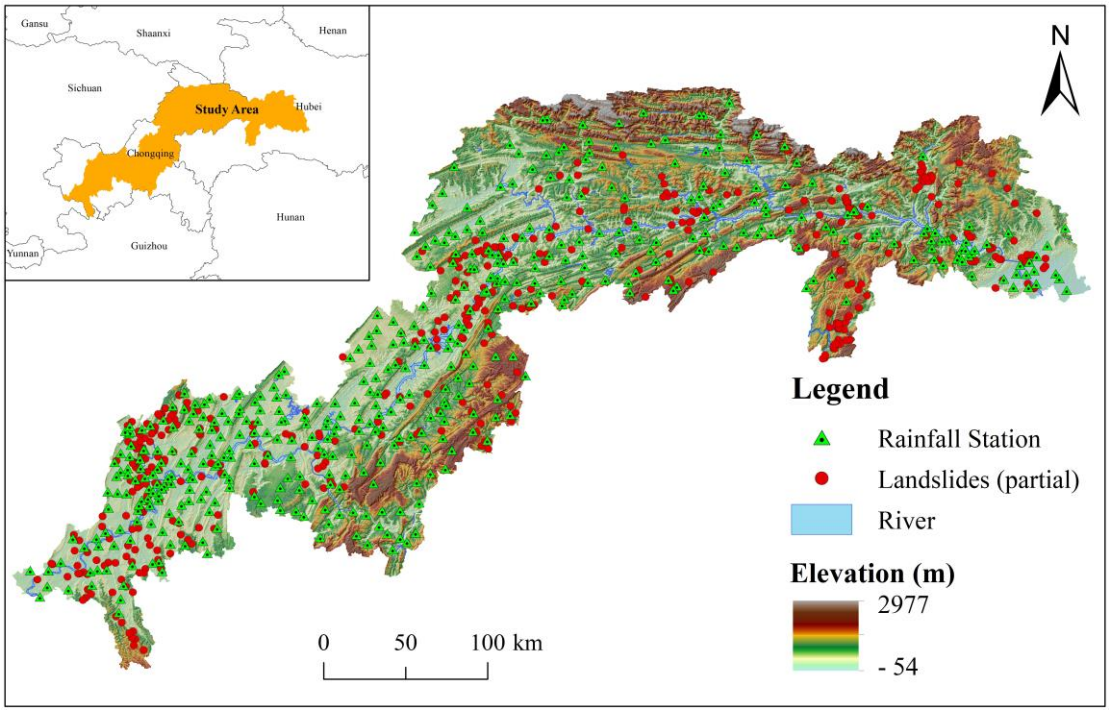

Figure 3: Geographic location of study area.

3.2 Study Area Subdivision and Landslide Data Cataloguing

Geomorphology, geology, and climate play the most important role in preparatory process of landslide initiation in any region (Dahal and Hasegawa, 2008), and the differences between them lead to different rainfall thresholds in various regions. Therefore, in this study, the whole study area was divided into 10 zones (Fig. 4) by considering the topography and climatic conditions of the study area, and the optimal RTM was calculated for each zone separately. Among them, Z_{11}, Z_{12} and Z_{13} are the moderate rainfall zone, low rainfall zone and high rainfall zone in the folded region; Z_{21}, Z_{22}, Z_{23}, Z_{24} and Z_{25} are the low rainfall zone, relatively high rainfall zone, high rainfall zone, moderate rainfall zone and high rainfall zone in the low

https://doi.org/10.5194/nhess-2024-109
Preprint. Discussion started: 19 July 2024

Natural Hazards and Earth System Sciences
Discussions

and medium mountain region, respectively; Z_3 is the high rainfall zone in the medium and high mountain region; and Z_4 is the high rainfall zone in the hilly and plain zone.

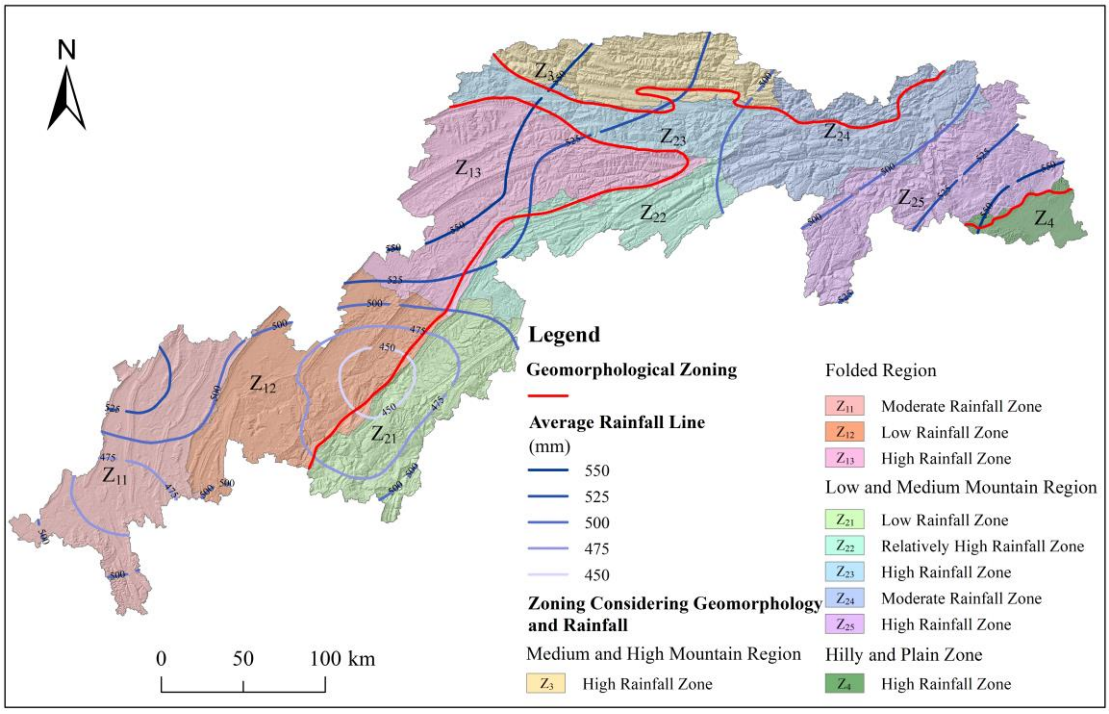

Figure 4: Zoning map of the study area.

Before landslide data cataloguing, the corresponding rainfall dataset needs to be acquired. Based on the abundance of rainfall stations in the study area (refer to Fig. 3, Rainfall Station), Thiessen polygon method were used for the delineation (Zhao et al., 2019), which facilitates the finding of rainfall stations corresponding to landslides. The Thiessen polygon method results satisfy the following conditions: (1) each polygon contains one and only one rainfall station; (2) any point within each polygon is the closest to the rainfall station within the unit; (3) the points on the boundary are the same distance to the two neighboring rainfall stations. The result of its division is shown in Fig. 5.

https://doi.org/10.5194/nhess-2024-109
Preprint. Discussion started: 19 July 2024

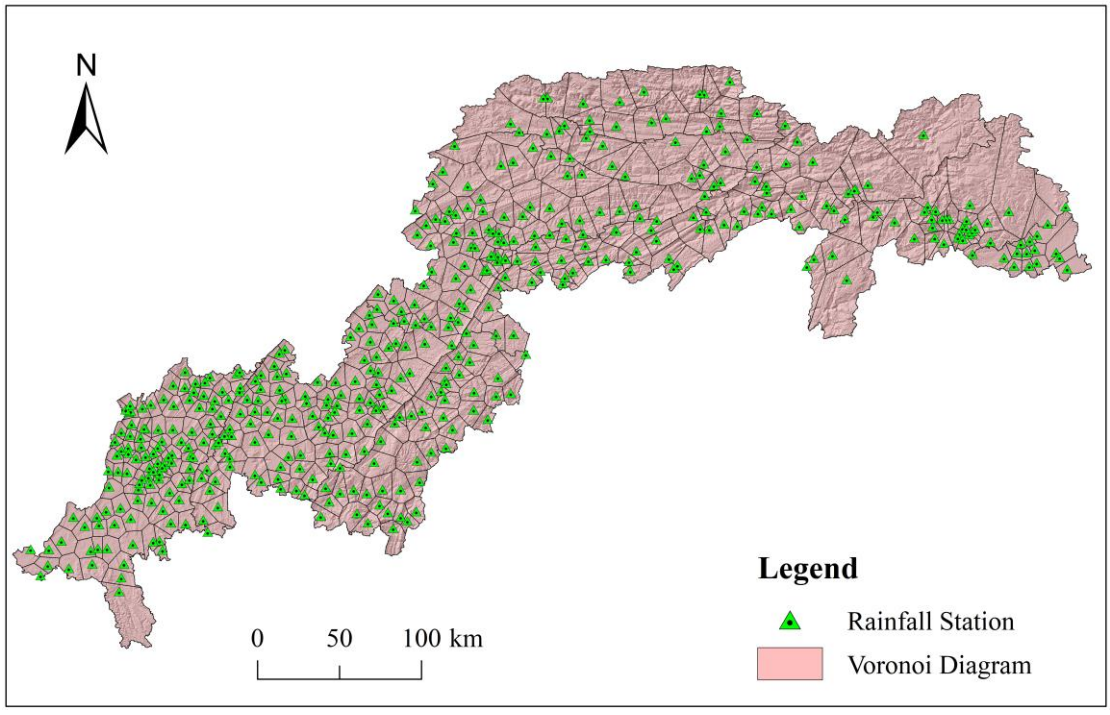

Figure 5: Thiessen polygon method results map.

Landslide data cataloguing is the basis for the study of rainfall thresholds (Gariano et al., 2021), and its main contents include basic information such as the time of occurrence of landslides, geographic location, associated rainfall stations, and so on. The landslide cataloguing data in this study were obtained from the historical landslide hazard data provided by Wuhan Geological Survey Centre (http://www.wuhan.cgs.gov.cn/).

A total of 453 historical landslides with precise rainfall information, particular dates, and places were acquired by aggregating historical landslide data, removing landslides with no rainfall and missing rainfall data (refer to Fig. 3, Landslide).

The rainfall in the study area is mainly concentrated from May to October, and the differences in climatic conditions between the dry and wet seasons might result in various impacts of rainfall on landslide movement (Soralump et al., 2021). Therefore, in this study, according to the time of occurrence of historical landslides, landslides occurring from May to October are classified as rainy season landslides, while landslides occurring from November to April are classified as dry season landslides. According to the records, there were 412 rainy season landslides and 41 dry season landslides (Fig. 6). Among them, rainfall thresholds for rainy season landslides were calculated separately according to the sub-districts; whereas the number of dry season landslides is small and further subdivision is not conducive to the calculation of rainfall thresholds, so only rainfall thresholds for dry season landslides were calculated for the entire study area.

https://doi.org/10.5194/nhess-2024-109
Preprint. Discussion started: 19 July 2024

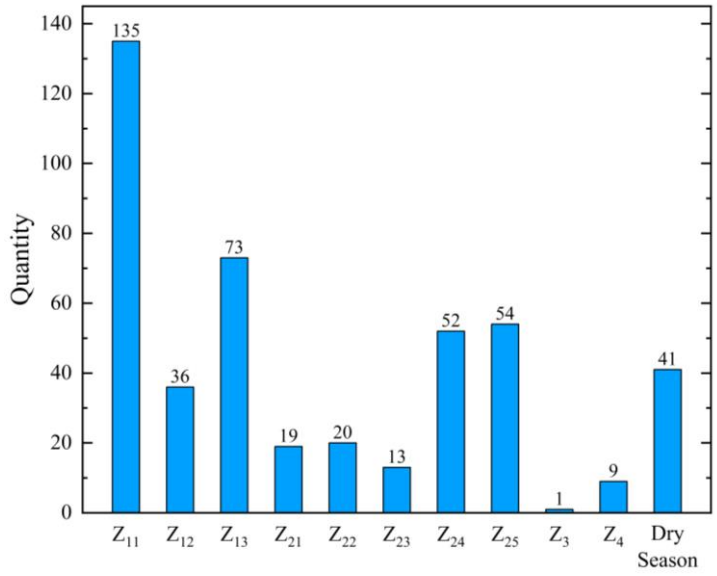

Figure 6: Number of landslides in each sub-district in the rainy season and the whole region in the dry season.

Figure 6 shows that the five zones Z_{21}, Z_{22}, Z_{23}, Z_3 and Z_4 have less catastrophe spots. To avoid insufficient data affecting rainfall threshold accuracy, this study merged some neighboring regions (Z_{21} and Z_{22} merged; Z_{23}, Z_{24}, and Z_3 merged; and Z_{25} and Z_4 merged) based on the geographic location of each region for rainfall threshold calculation.

4. Results

4.1 Rainfall Threshold Model Results

4.1.1 E-D Rainfall Threshold Model

Rainfall-triggered landslide is a random and small probability event, and if only the minimum threshold is used to warn of geological hazards, it will produce many ineffective warnings (i.e., False Positive Error) (Sarkar et al., 2023). While decreasing the public's trust in disaster warning, it will result in a waste of resources for preventive and control activities, which is not favorable to the advancement of disaster prevention and mitigation. Therefore, most of the current studies on RTM use a variety of threshold curves with different landslide probabilities (Sheng et al., 2022), in order to improve the reasonableness and accuracy of rainfall warning. Generally, the landslide probability indicates the proportion of the number of landslides triggered by rainfall exceeding a certain threshold among all occurring landslides (Yang et al., 2020).

In the calculation of OLS regression, the E and D scatters of historical landslide hazard locations in each area were first plotted into the E-D log-log coordinates system, and the 50% landslide probability rainfall threshold curve was derived by fitting using OLS regression. The fitted curves were then used to run OLS regression analysis on the historical landslide hazard points above and below the curves to get the 75% landslide probability rainfall threshold curve and the 25% landslide

https://doi.org/10.5194/nhess-2024-109
Preprint. Discussion started: 19 July 2024

Natural Hazards and Earth System Sciences
Discussions

190 probability rainfall threshold curve (Fig. 7). Finally, the log-log coordinates system straight lines were transformed to Cartesian coordinate system curves (Table 1).

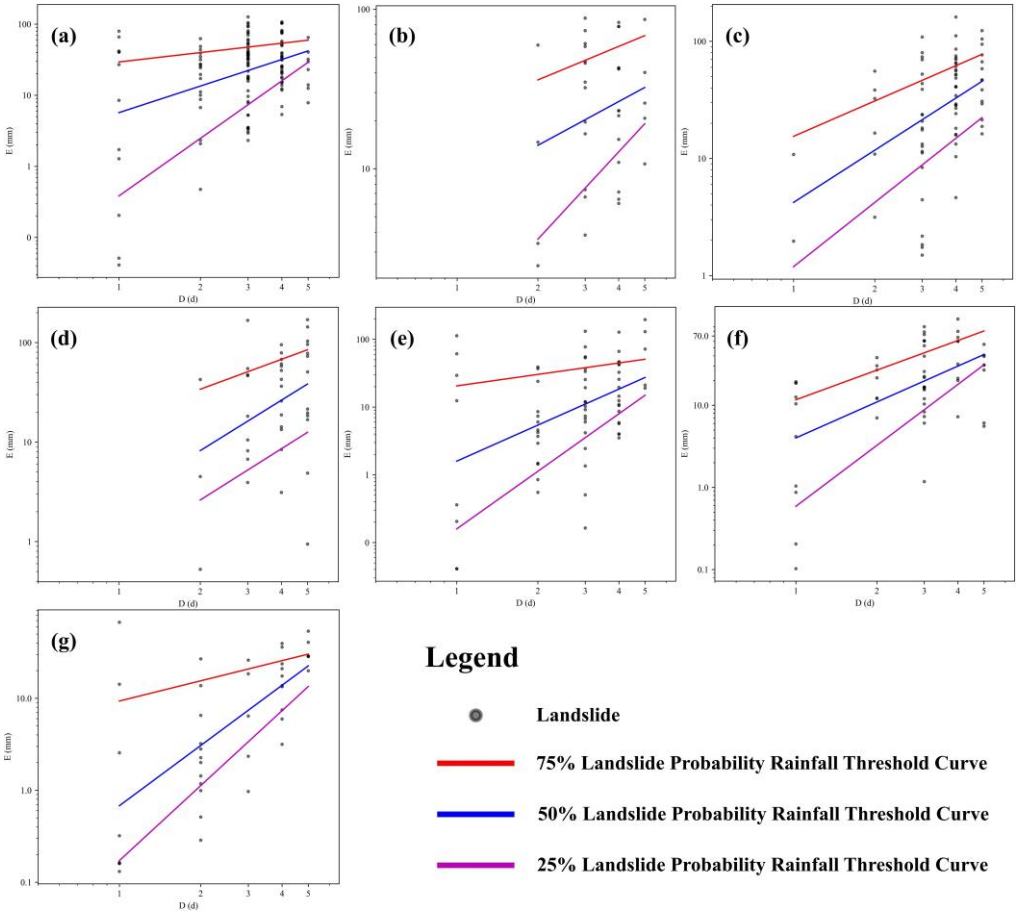

Figure 7: Plot of E-D rainfall threshold model results in log-log coordinates system (OLS regression). In the figure, a is the Z_{11} region, b is the Z_{12} region, c is the Z_{13} region, d is the $Z_{21}Z_{22}$ region, e is the $Z_{23}Z_{24}Z_3$ region, f is the $Z_{25}Z_4$ region, and g is the Dry
195 **Season**

Table 1: E-D rainfall threshold equation (OLS regression).

Region	Landslide probability	Equations (Log-log coordinates system)	E-D equation
Z_{11}	75%	y=0.4383x+1.4679	$E=29.3697\times D^{0.4383}$
	50%	y=1.2420x+0.7552	$E=5.6912\times D^{1.2420}$
	25%	y=2.6894x-0.4164	$E=0.3834\times D^{2.6894}$
Z_{12}	75%	y=0.6981x+1.3464	$E=22.2024\times D^{0.6981}$
	50%	y=0.9113x+0.8721	$E=7.4490\times D^{0.9113}$
	25%	y=1.8193x+0.0102	$E=1.0238\times D^{1.8193}$

https://doi.org/10.5194/nhess-2024-109
Preprint. Discussion started: 19 July 2024

Z_{13}	75%	y=1.0019x+1.1887	$E=15.4419\times D^{1.0019}$
	50%	y=1.4792x+0.6246	$E=4.2131\times D^{1.4792}$
	25%	y=1.8201x+0.0759	$E=1.1910\times D^{1.8201}$
$Z_{21}Z_{22}$	75%	y=0.9977x+1.2307	$E=17.0098\times D^{0.9977}$
	50%	y=1.6825x+0.4075	$E=2.5556\times D^{1.6825}$
	25%	y=1.7100x-0.0969	$E=0.8000\times D^{1.7100}$
$Z_{23}Z_{24}Z_{3}$	75%	y=0.5633x+1.3125	$E=20.5353\times D^{0.5633}$
	50%	y=1.7673x+0.2014	$E=1.5900\times D^{1.7673}$
	25%	y=2.8230x-0.7986	$E=0.1590\times D^{2.8230}$
$Z_{25}Z_{4}$	75%	y=1.1974x+1.0675	$E=11.6815\times D^{1.1974}$
	50%	y=1.4525x+0.6027	$E=4.0059\times D^{1.4525}$
	25%	y=2.4652x-0.2305	$E=0.5882\times D^{2.4652}$
Dry Season	75%	y=0.7295x+0.9706	$E=9.3454\times D^{0.7295}$
	50%	y=2.1754x-0.1679	$E=0.6794\times D^{2.1754}$
	25%	y=2.7079x-0.7646	$E=0.1719\times D^{2.7079}$

In the calculation of MLP regression, the rainfall thresholds corresponding to 50% landslide probability for each duration of rainfall (D) were first fitted separately. The MLP regression was then performed on the historical landslide data above and below the thresholds, respectively, to obtain the 75% landslide probability and 25% landslide probability rainfall thresholds corresponding to each D. Due to the lack of historical landslide hazard data at a D of 1 in some regions (e.g., region Z_{12}) and the small amount of historical landslide hazard data at a D of 5 in some regions (e.g., region Z_{11}), these can lead to irrational results of the fitted rainfall thresholds. In this regard, this study used Gaussian regression (Kumar and Kavitha, 2021) and GM(1,1) grey prediction model (Chen and Huang, 2013) to correct the rainfall threshold results obtained from MLP regression. The corrected results are shown in Fig. 8 and Table 2.

https://doi.org/10.5194/nhess-2024-109
Preprint. Discussion started: 19 July 2024

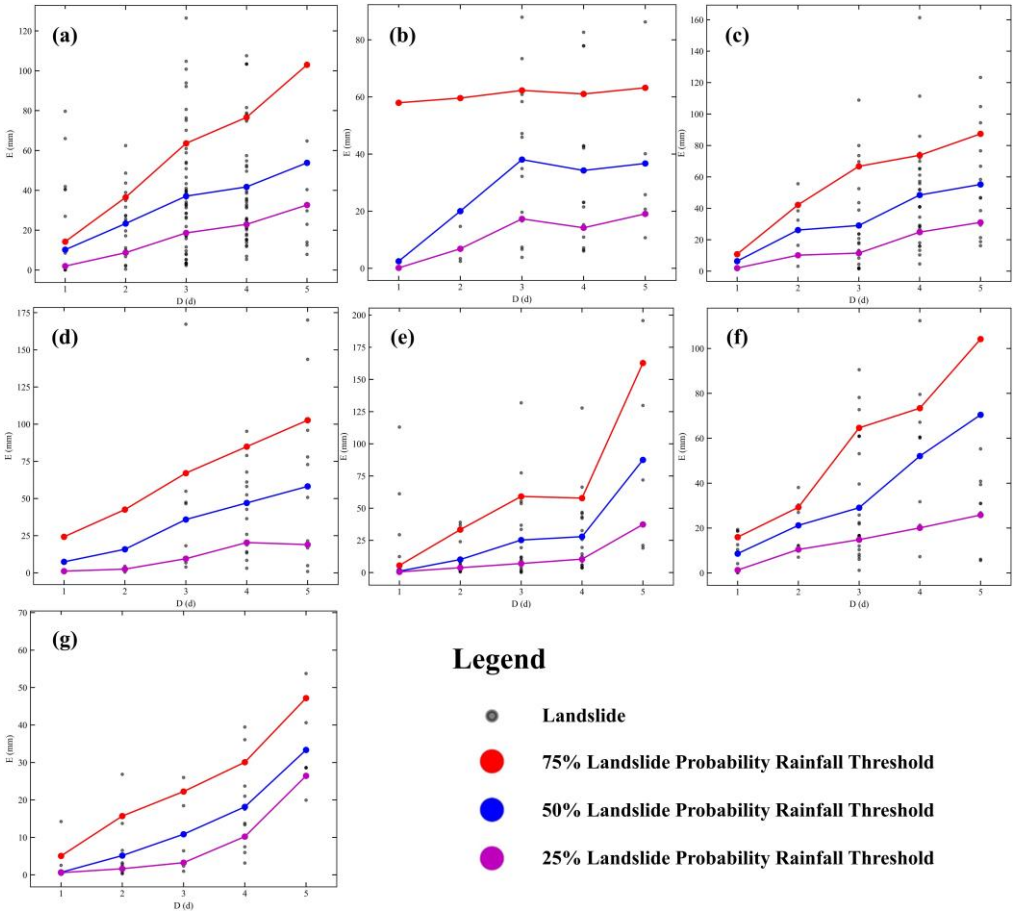

Figure 8: Plot of E-D rainfall threshold model results (MLP regression). In the figure, a is the Z_{11} region, b is the Z_{12} region, c is the Z_{13} region, d is the $Z_{21}Z_{22}$ region, e is the $Z_{23}Z_{24}Z_3$ region, f is the $Z_{25}Z_4$ region, and g is the Dry Season

The red, blue, and purple points in Fig. 8 are the rainfall threshold points obtained from the fit for different landslide probabilities. The line segments are just for connecting the individual threshold points for viewing purposes and have no

Table 2: E-D rainfall threshold (MLP regression).

Region	Duration of rainfall (D)	75% threshold (mm)	50% threshold (mm)	25% threshold (mm)
Z_{11}	1	14.2305	10.1800	1.9625
	2	36.4914	23.3267	8.7024
	3	63.5907	37.0893	18.6210
	4	76.6291	41.7210	22.9260
	5	103.0000	53.8090	32.6260
Z_{12}	1	57.9690	2.4749	0.1550
	2	59.6126	20.0312	6.8458
	3	62.3002	38.0666	17.3107

https://doi.org/10.5194/nhess-2024-109
Preprint. Discussion started: 19 July 2024


Natural Hazards and Earth System Sciences
Discussions

	4	61.0451	34.2639	14.1966
	5	63.2107	36.7170	19.0748
Z_{13}	1	10.8122	6.3897	1.9677
	2	42.1870	26.1761	10.1656
	3	66.7259	29.0723	11.5028
	4	73.7542	48.4590	24.8502
	5	87.3909	55.1944	31.0476
$Z_{21}Z_{22}$	1	24.2575	7.4117	1.1585
	2	42.5658	15.8642	2.5160
	3	67.0825	35.8785	9.5152
	4	84.8807	47.0166	20.3769
	5	102.6789	58.1546	18.9942
$Z_{23}Z_{24}Z_3$	1	5.5210	1.0893	0.5702
	2	33.3538	10.1252	3.7901
	3	59.1386	25.2715	7.0353
	4	57.8357	27.9044	10.4444
	5	162.7467	87.5204	37.3694
$Z_{25}Z_4$	1	15.9482	8.6114	1.2742
	2	29.2418	21.1900	10.4545
	3	64.6284	29.0526	14.8209
	4	73.3920	52.0651	20.0756
	5	104.1990	70.4430	25.8100
Dry Season	1	5.0503	0.6647	0.5818
	2	15.7035	5.1495	1.6332
	3	22.2420	10.8428	3.2452
	4	30.0733	18.1523	10.2084
	5	47.1948	33.3588	26.4428

The threshold curves generated from OLS regression in the log-log coordinates system often exhibit an upward trend, as shown in Fig. 7, and the slopes of the rainfall threshold curves for 25%, 50%, and 75% landslide probability gradually decrease. From Fig. 8, the rainfall thresholds obtained from MLP regression for different landslide probabilities also show a generally increasing trend, but the relatively small amount of historical landslide data in some subregions results in relatively unreasonable rainfall thresholds (e.g., the rainfall threshold for the $Z_{23}Z_{24}Z_3$ region shows a large increase when D is 5).

4.1.2 E-D-R Rainfall Threshold Model

Based on the above E-D rainfall threshold model, the third dimension indicator R was introduced to construct the E-D-R rainfall threshold model. In this model, the value of R is taken equal to the rainfall threshold corresponding to when D is 1 in the E-D RTM. These three indicators visually form a closed "box" (Fig. 9), with "nested" relationships between the different landslide probability levels.

https://doi.org/10.5194/nhess-2024-109
Preprint. Discussion started: 19 July 2024

Natural Hazards and Earth System Sciences
Discussions

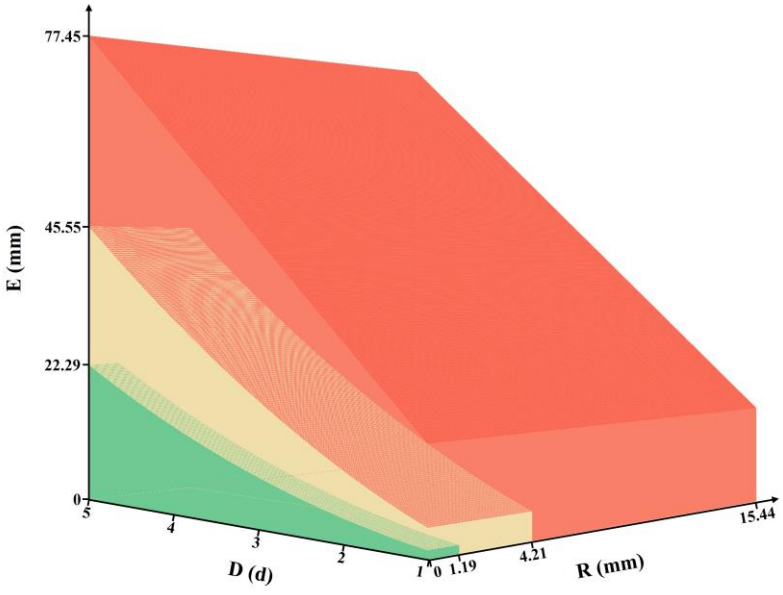

Figure 9: Schematic of the E-D-R rainfall threshold model obtained from the OLS regression (Z_{13}).

In Fig. 9, the green, yellow, and red boxes indicate rainfall thresholds of <25%, 25-50% and 50-75% landslide probability, respectively.

4.1.3 Model Accuracy Verification

The accuracy of the model was tested in this research utilizing 82 landslide hazards events that were not involved in the RTM calculations in 2019 and 2020. Figure 10 depicts the number of landslide hazards events in each region.

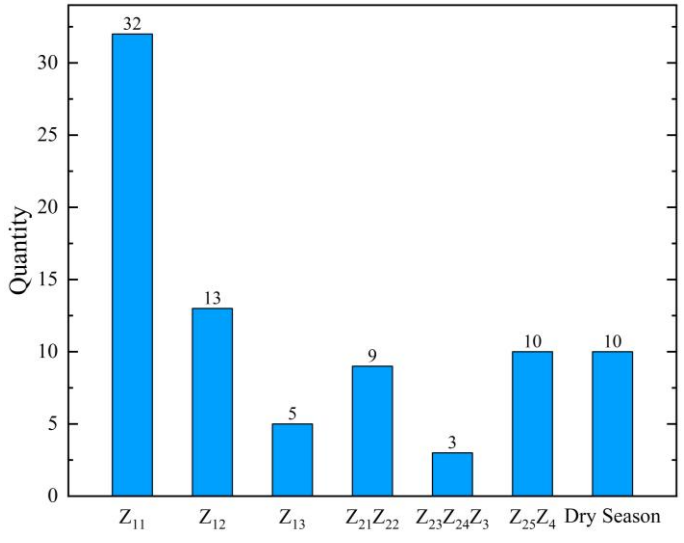

Figure 10: The number of landslide hazard events in each region of the validation set.

https://doi.org/10.5194/nhess-2024-109
Preprint. Discussion started: 19 July 2024

230 In the actual landslide control work, it is impossible to obtain the real rainfall on a certain day in the future, so it can only be replaced by the forecast rainfall. In order to make the validation data source of the rainfall threshold model more realistic, this study relies on the abundant rainfall forecasting stations in the study area (Fig. 11) and counts the forecast rainfall on the day of the occurrence of these 82 landslide hazards as well as the previous 5 days for the validation of the model.

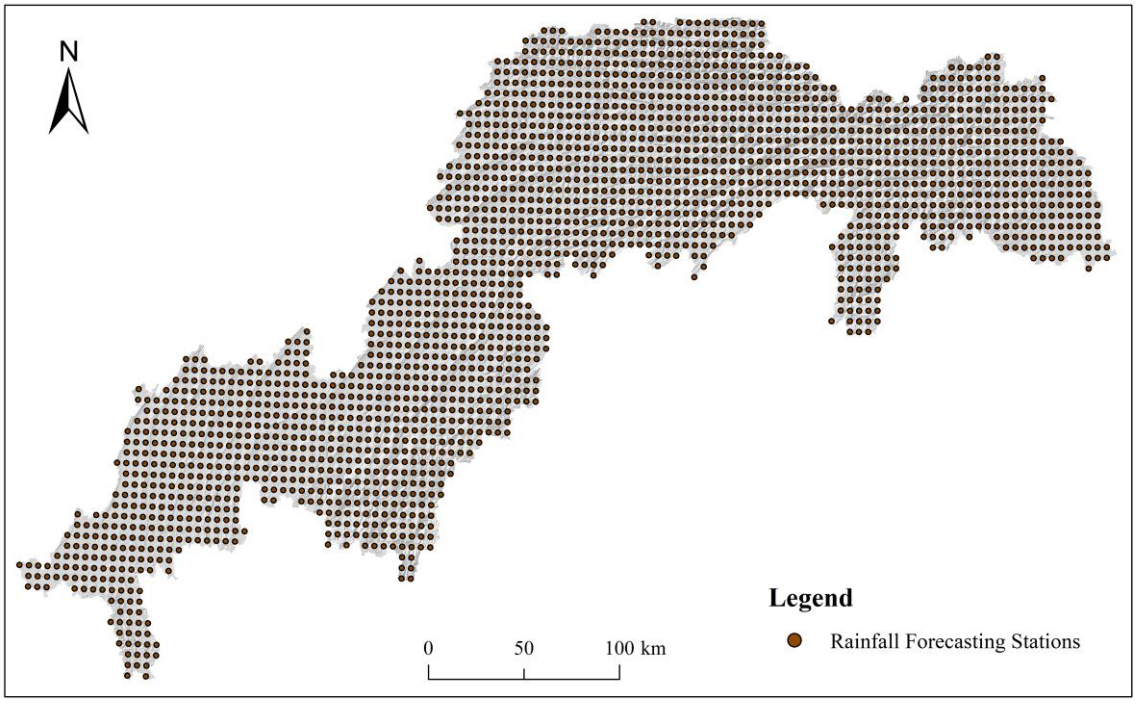

235 **Figure 11: Map of rainfall forecasting stations.**

The rainfall forecast stations in Fig. 11 are distributed at 0.05° intervals, and the forecast rainfall data were provided by the Wuhan Geological Survey Centre. The data are updated in real time according to meteorological changes, and the data used in the study are adopted from the latest update of the forecast data to ensure the accuracy of the data.

The research region was classified into four warning categories based on the rainfall threshold classification results: attention
240 (<25%), special attention (25-50%), warning (50%-75%), and severe warning (≥75%). Figure 12 displays the ultimate outcomes of the validation process for each region's four RTM categories. Furthermore, Table 3 displays the proportion of hazardous circumstances corresponding to the two warning levels of “severe warning” and “warning” in the E-D-R RTM validation results.

https://doi.org/10.5194/nhess-2024-109
Preprint. Discussion started: 19 July 2024

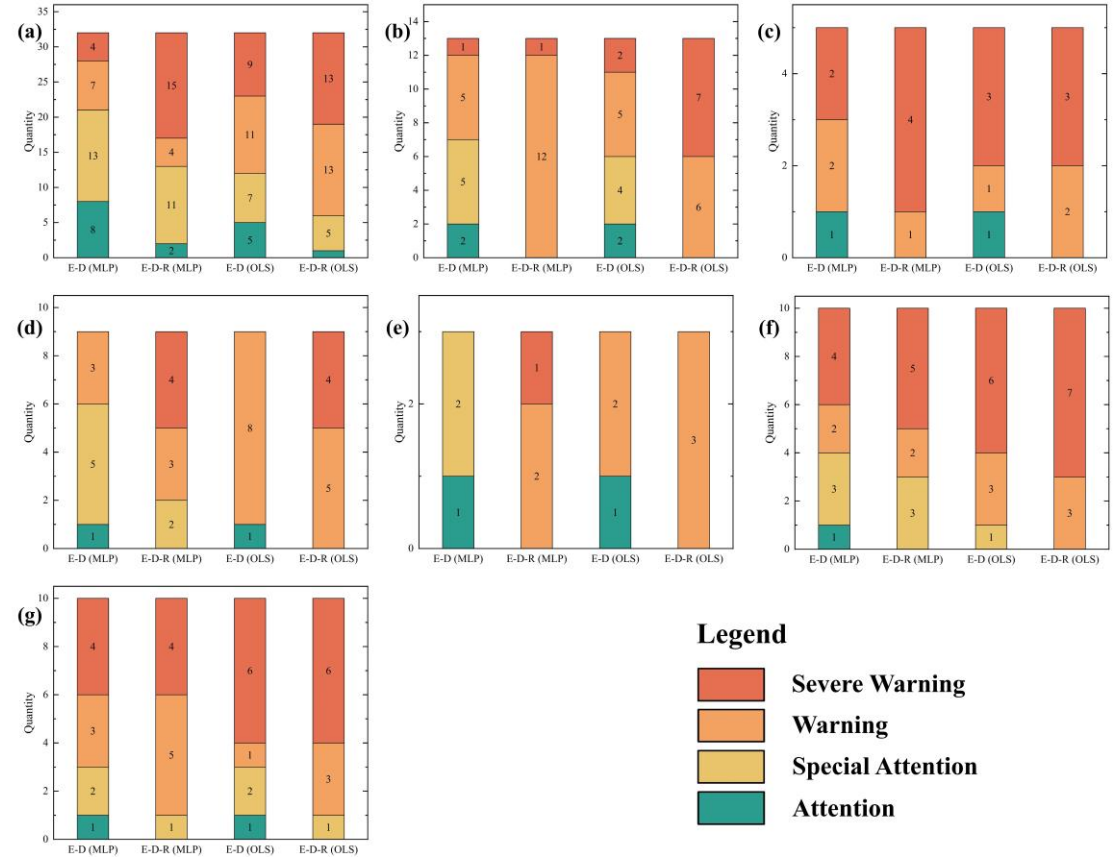

Figure 12: The distribution of warning levels in the validation set for each partitioned region. In the figure, a is the Z_{11} region, b is the Z_{12} region, c is the Z_{13} region, d is the $Z_{21}Z_{22}$ region, e is the $Z_{23}Z_{24}Z_3$ region, f is the $Z_{25}Z_4$ region, and g is the Dry Season

Table 3: Proportion of hazard events corresponding to the "Severe Warning" and "Warning" levels in the E-D-R RTM for each partitioned region.

Region	Regression approach	Level	Percentage (%)
Z_{11}	MLP	Severe Warning	46.88
		Warning	12.50
	OLS	Severe Warning	40.63
		Warning	40.63
Z_{12}	MLP	Severe Warning	7.69
		Warning	92.31
	OLS	Severe Warning	53.85
		Warning	46.15
Z_{13}	MLP	Severe Warning	80.00
		Warning	20.00
	OLS	Severe Warning	60.00
		Warning	40.00

https://doi.org/10.5194/nhess-2024-109
Preprint. Discussion started: 19 July 2024


Natural Hazards and Earth System Sciences Discussions

$Z_{21}Z_{22}$	MLP	Severe Warning	44.44
		Warning	33.33
	OLS	Severe Warning	44.44
		Warning	55.56
$Z_{23}Z_{24}Z_3$	MLP	Severe Warning	33.33
		Warning	66.67
	OLS	Severe Warning	0.00
		Warning	100.00
$Z_{25}Z_4$	MLP	Severe Warning	50.00
		Warning	20.00
	OLS	Severe Warning	70.00
		Warning	30.00
Dry Season	MLP	Severe Warning	40.00
		Warning	50.00
	OLS	Severe Warning	60.00
		Warning	30.00

The following conclusions may be drawn from an analysis of the prediction accuracy of the four categories of RTM:

(1) The accuracies of the E-D-R RTM computed using MLP regression and OLS regression are much better than the comparable E-D RTM. The E-D-R RTM predict outputs no longer include the "Attention" warning level for all areas (Z11 excepted) when the R indicator was included in the third dimension. Furthermore, there has been a rise in the percentage of hazard incidents categorized as "Warning" and "Severe Warning" categories across all regions. Compared with the E-D model, the proportion of hazardous conditions in the "Warning" and "Severe Warning" warning levels of the E-D-R RTM increases from 41.46% to 76.82%, and the result of OLS regression increases from 69.51% to 91.46%.

(2) The prediction accuracies of the E-D-R RTM for each region are slightly different between the MLP regression and the OLS regression, but in general, the total proportion of hazardous conditions at the warning levels of "Warning" and "Severe Warning" is similar.

(3) The optimal RTM for each region is shown in Table 4.

Table 4: Optimal RTM for each partitioned region.

Region	Optimal rainfall threshold modelling (regression approach)
Z_{11}	E-D-R (OLS)
Z_{12}	E-D-R (OLS)
Z_{13}	E-D-R (MLP)
$Z_{21}Z_{22}$	E-D-R (OLS)
$Z_{23}Z_{24}Z_3$	E-D-R (MLP)

https://doi.org/10.5194/nhess-2024-109
Preprint. Discussion started: 19 July 2024

$Z_{25}Z_4$	E-D-R (OLS)
Dry Season	E-D-R (OLS)

The optimal RTM for Z_{13} and $Z_{23}Z_{24}Z_3$ regions are the E-D-R models obtained from the MLP regression, proving the feasibility of using neural networks (MLP) for RTM research.

4.2 Landslide Susceptibility Results

4.2.1 Landslide Inducing Factor Selection

Combined with the research results of previous scholars (Chen et al., 2021; Chen et al., 2020; Habumugisha et al., 2022; Li et al., 2022; Rohan et al., 2023) and the actual situation of the study area, a total of 11 landslide inducing factors, including elevation, Normalized Difference Vegetation Index (NDVI), Topographic Wetness Index (TWI), road density, stratigraphic lithology, tectonic density, river distance, slope, curvature, land cover, and slope structure, were selected in this study.

Table 5 shows the data sources for these 11 factors.

Table 5: Source of data on landslide inducing factors.

Factor Category	Data Source	Inducing Factor
Topography and Geomorphology	Geological Map STRM DEM (30m)	Elevation Slope Curvature Slope Structure
Geological Lithology	Geological Map	Stratigraphic Lithology Tectonic Density
Hydrological Factor	National Basic Geographic Database STRM DEM (30m)	TWI River Distance
Land Use	Landsat Remote Sensing Image (30m)	NDVI Land Cover Type
Human Engineering Activities	OpenStreetMap	Road Density

Among them, the slope structure considers the relationship between the slope aspect of the slope and the inclination of the rock formation (Niu et al., 2014), and different types of slope structures can lead to differences in landslide size and intensity. Based on different slope gradient (σ), slope direction (γ), and inclination (α) and tendency (β) of the rock formation, the following eight types of slope structures are classified (Table 6).

Table 6: Classification of slope structure types and percentage of each type in the study area.

Code	Relationship between α, β, γ and σ	Area (%)
A	$\alpha \leq 5°$	1.720
B	$\alpha > 5°$, $\lvert\gamma-\beta\rvert \in [0°, 30°)$ or $\lvert\gamma-\beta\rvert \in [330°, 360°)$, $\sigma > \alpha$	5.127

https://doi.org/10.5194/nhess-2024-109
Preprint. Discussion started: 19 July 2024

Natural Hazards and Earth System Sciences
Discussions

C	α>5°, |γ-β|∈[0°, 30°) or |γ-β|∈[330°, 360°), σ=α	0.000
D	α>5°, |γ-β|∈[0°, 30°) or |γ-β|∈[330°, 360°), σ<α	13.581
E	α>5°, |γ-β|∈[30°, 60°) or |γ-β|∈[300°, 330°)	17.559
F	α>5°, |γ-β|∈60°, 120°) or |γ-β|∈[240°, 300°)	32.066
G	α>5°, |γ-β|∈[120°, 150°) or |γ-β|∈[210°, 240°)	15.089
H	α>5°, |γ-β|∈[150°, 210°)	14.857

Stratigraphic lithology data was obtained by vectorizing and classifying geological maps (scale 1:200,000). Each lithology has a different pedogenic environment and will vary in composition and stability, which affects the occurrence of landslides (Cobos-Mora et al., 2023). In this paper, the study area is classified into four categories: carbonate, clastic, carbonate and clastic, as well as Igneous and metamorphic rocks. In addition, when the research area is large and most of the tectonics are intertwined with each other, the distance from tectonics is no longer suitable as a correlation factor, and tectonic density should be used instead (Wang et al., 2014). Also, since the road data also show interlocking status, this paper uses tectonic density and road density as evaluation factors. When using ArcGIS to calculate the density, the search radius is kept as default, and the area unit is square kilometers.

To ensure the reasonableness of the selection of landslide inducing factors, this study used Pearson correlation analysis to explore the degree of correlation among the selected inducing factors (Zhang et al., 2022) (Fig. 13). The value of correlation ranges from -1 to 1. The closer the value is to 1 or -1, the stronger the correlation between the two variables, and the closer the value is to 0, the weaker the correlation between the two variables (Cao et al., 2023).

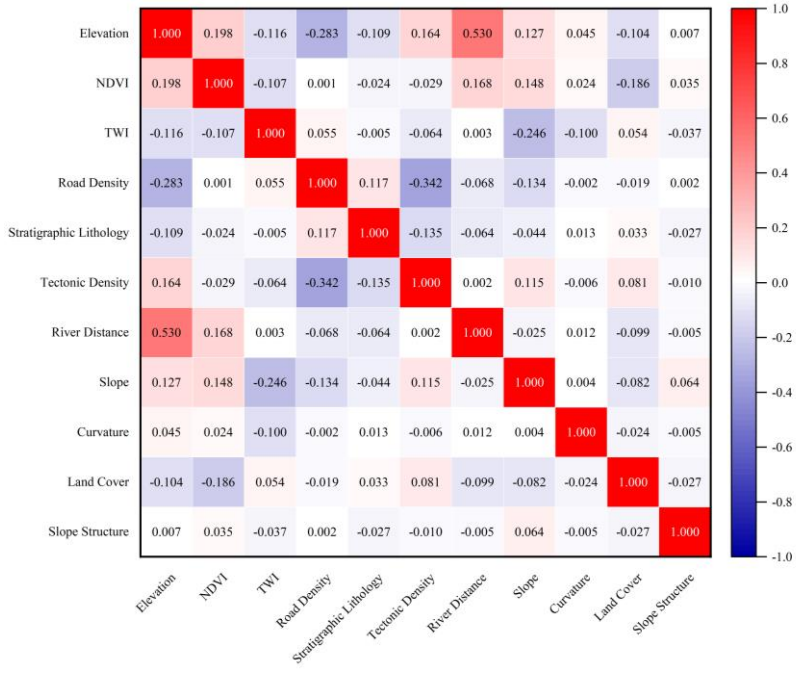

Figure 13: Pearson correlation results for inducing factors.

https://doi.org/10.5194/nhess-2024-109
Preprint. Discussion started: 19 July 2024

The correlation coefficients between the inducing factors are low, as shown in Fig. 13, with the exception of the somewhat higher correlation value between elevation and river distance (0.53). Given that elevation and river distance are two important factors for causing landslides (elevation is inherent in the assessment of LS (Wang et al., 2022b), which affects the distribution of submerged layers as well as the intensity of human activities; and the erosive effect of the river on the shoreline can damage the foot of the slope and soften the rock and soil mass (Selamat et al., 2022)), they are all retained in this study. These 11 inducing factors were finally determined to be used in the TGRA's LS assessment research.

4.2.2 Grading of Landslide Susceptibility Factors

Combined with the actual situation of the study area and the results of previous studies, the class classification of each landslide predisposing factor and the result map of this study are shown in Table 7 and Fig. 14. The susceptibility evaluation was carried out in raster cells with a size of 30m × 30m. It's also worth noting that the historical landslide data utilized for LS prediction includes all 6,888 recorded landslides, not just the 453 filtered for inclusion in the RTM calculations.

Table 7: Classification of landslide inducing factors.

Predisposing Factor	Classification Criteria	Code
Elevation (m)	≤300 (300,600] (600,900] (900,1200] (1200,1500] >1500	a
NDVI	[-1,0] (0,0.2] (0.2,0.4] (0.4,0.6] (0.6,0.8] (0.8,1]	b
TWI	≤6 (6,8] (8,10] (10,14] >14	c
Road Density	[0,0.5] (0.5,1.2] (1.2,2.5] (2.5,5.0] >5.0	d

https://doi.org/10.5194/nhess-2024-109
Preprint. Discussion started: 19 July 2024


Natural Hazards and Earth System Sciences
Discussions

Stratigraphic Lithology	Carbonates Clastic rocks Carbonates and clastic rocks Igneous and metamorphic rocks	e
Tectonic Density	[0,0.03] (0.03,0.12] (0.12,0.24] (0.24,0.38] >0.38	f
River Distance (m)	≤500 (500,1000] (1000,1500] >1500	g
Slope (°)	[0,10] (10,20] (20,30] (30,40] (40,50] >50	h
Curvature	≤-3 (-3,-1] (-1,0] (0,1] >1	i
Land Cover	Urban land Agricultural land Forest land Grassland Water Other Land	j
Slope Structure	A B D E F G H	k

https://doi.org/10.5194/nhess-2024-109
Preprint. Discussion started: 19 July 2024

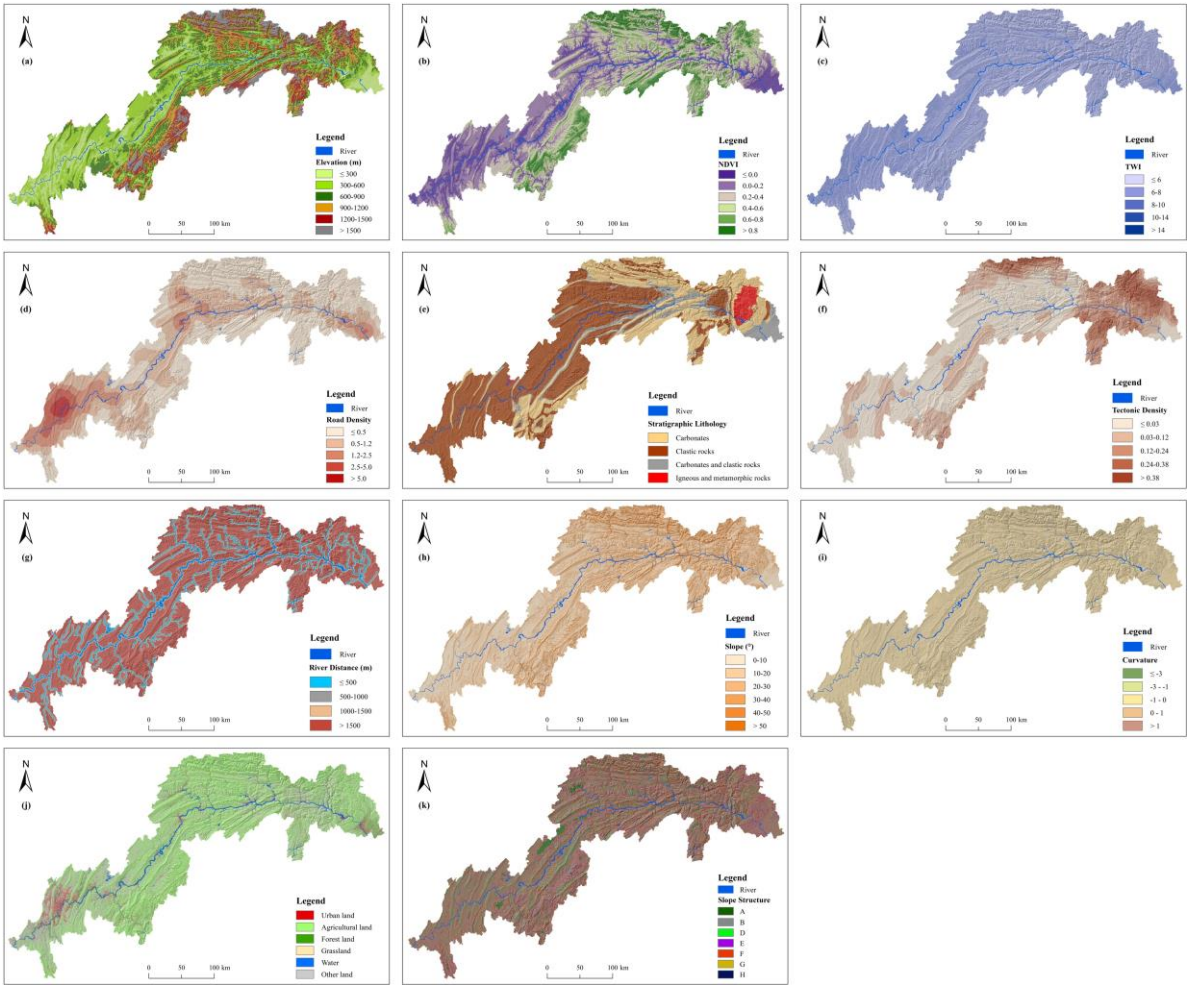

Figure 14: Landslide inducing factors grading results map.

4.2.3 Landslide Susceptibility Evaluation Results

In this study, three models, CNN-3D, RF and SVM, were used to evaluate the LS of the study area, and the optimal LS result was chosen for subsequent daily LHW. The relevant indicators obtained from the training of the three models are shown in Table 8.

Table 8: Results of the training of the susceptibility evaluation model.

Model	Model Evaluation Indicators				
	AUC	Accuracy	Precision	Recall	F1_score
CNN-3D	0.96	0.9003	0.8663	0.9295	0.8968
RF	0.82	0.7500	0.7656	0.7416	0.7534
SVM	0.83	0.7630	0.7625	0.7623	0.7624

https://doi.org/10.5194/nhess-2024-109
Preprint. Discussion started: 19 July 2024

Natural Hazards and Earth System Sciences
Discussions

Table 8 shows that the AUC values for CNN-3D, RF, and SVM models are 0.96, 0.82, and 0.83, respectively. The AUC values indicate that all three models can better predict the probability of landslide occurrence in the study area, but the CNN-3D model has a greater prediction accuracy than the RF and SVM models. In addition, for the other four metrics, the CNN-3D model outperforms the RF and SVM models. As a consequence, in this study, the CNN-3D model's LS result was divided into five classes using the natural breaks approach (Fig. 15) and was used for subsequent daily LHW.

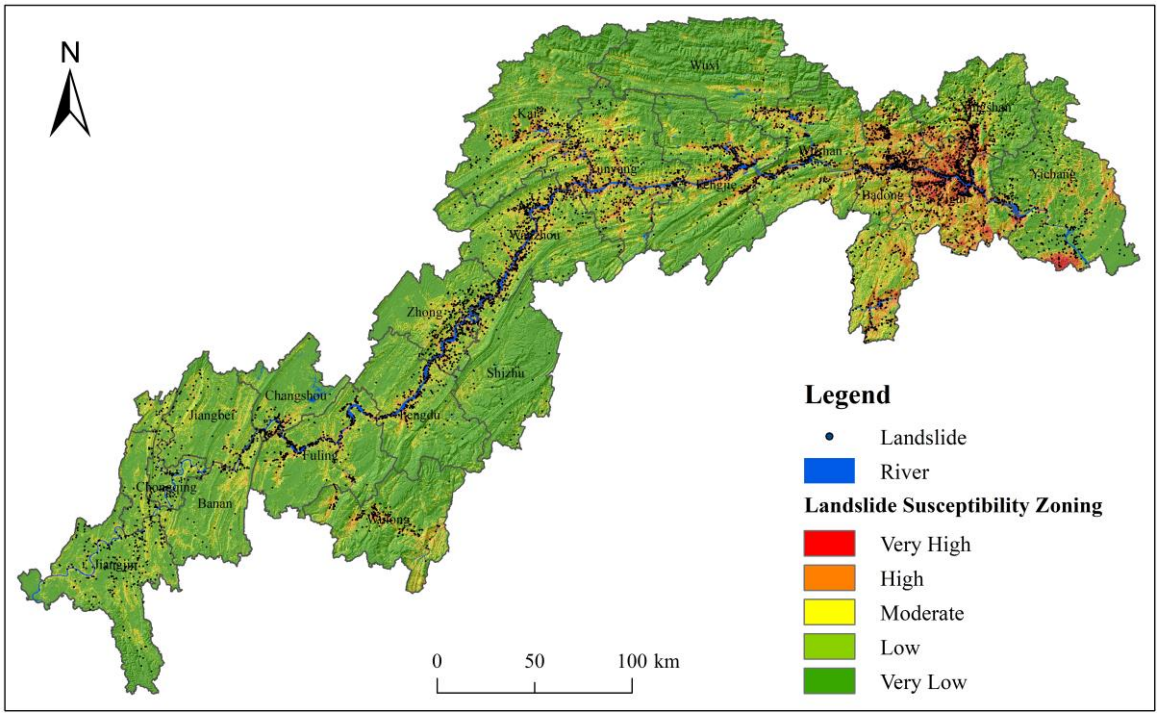

Figure 15: CNN-3D model landslide susceptibility results.

As a whole, the landslide disaster high susceptibility areas in the study area are mainly concentrated along the riverbanks and in the central and eastern regions. In terms of district and county scopes, the landslide disaster high susceptibility areas are mainly concentrated at Zigui, the northern part of Badong, the southern part of Xingshan, the central part of Fengjie, the central part of Wanzhou, and the southeastern part of Zhongxian.

4.3 Landslide Hazard Warning

4.3.1 Landslide Hazard Results for Each Rainfall Warning Level

In this study, a superposition matrix (Table 9) was created to couple the daily RWL with the LS result to generate the daily LHW result. Based on the superimposed matrix, four categories of landslide hazard levels will be obtained, where 1 indicates relatively stable zone, 2 indicates general prevention zone, 3 indicates secondary prevention zone, and 4 indicates priority prevention zone.

https://doi.org/10.5194/nhess-2024-109
Preprint. Discussion started: 19 July 2024

Natural Hazards and Earth System Sciences
Discussions

Table 9: Landslide susceptibility and rainfall warning level superposition matrix.

Rainfall Threshold Level \ Susceptibility	Very Low	Low	Moderate	High	Very High
Caution	1	1	1	1	2
Special Caution	1	1	1	2	3
Warning	1	1	2	3	4
Severe Warning	1	2	3	4	4

Based on the LS results shown in Fig. 15, combined with Table 9, the LHW results corresponding to each rainfall level were obtained (Fig. 16).

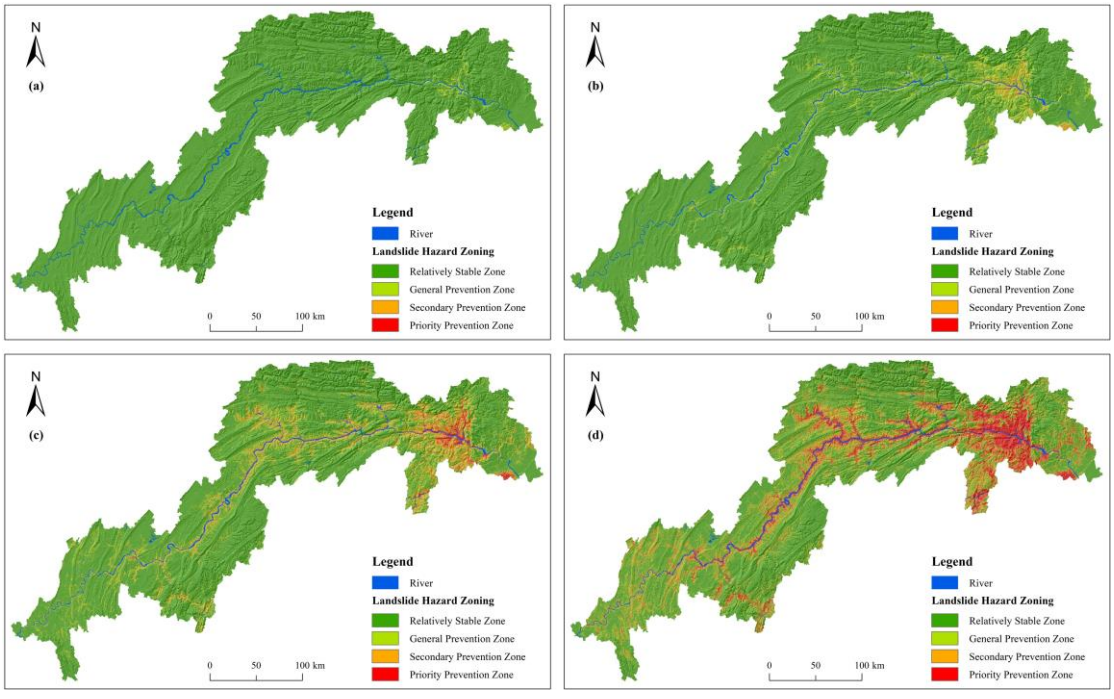

Figure 16: Landslide hazard maps for each rainfall warning level. (a. attention level hazard; b. special attention level hazard; c. warning level hazard; d. severe warning level hazard).

4.3.2 Daily Landslide Hazard Warning

In 2020, the Yangtze River experienced its worst basin-wide flood since 1998. on July 19, the "Yangtze River Flood No. 2 of 2020" was progressing through the TGRA to the middle and lower reaches of the Yangtze River, and the persistent rainfall induced many landslides. Therefore, in this study, 19 July 2020 was used as an example for LHW and validation. Based on the anticipated rainfall data at the time, E and D for the rainfall forecast stations from 14 July 2020 to 18 July 2020, and R for 19 July 2020, were calculated. Kriging interpolation was used to generate E (Fig. 17.a) and R (Fig. 17.b) for the whole research region. Since D is an integer ranging from 0 to 5, interpolation cannot be used to acquire D for the whole research

https://doi.org/10.5194/nhess-2024-109
Preprint. Discussion started: 19 July 2024

Natural Hazards and Earth System Sciences
Discussions

region; thus, this study uses the Thiessen polygon method and feature to raster method to obtain D for the entire study area (Fig. 17.c).

The RWL for 19 July 2020 was calculated per sub-region (Fig. 17.d) using the optimum RTM for each sub-region obtained above (Table 4).

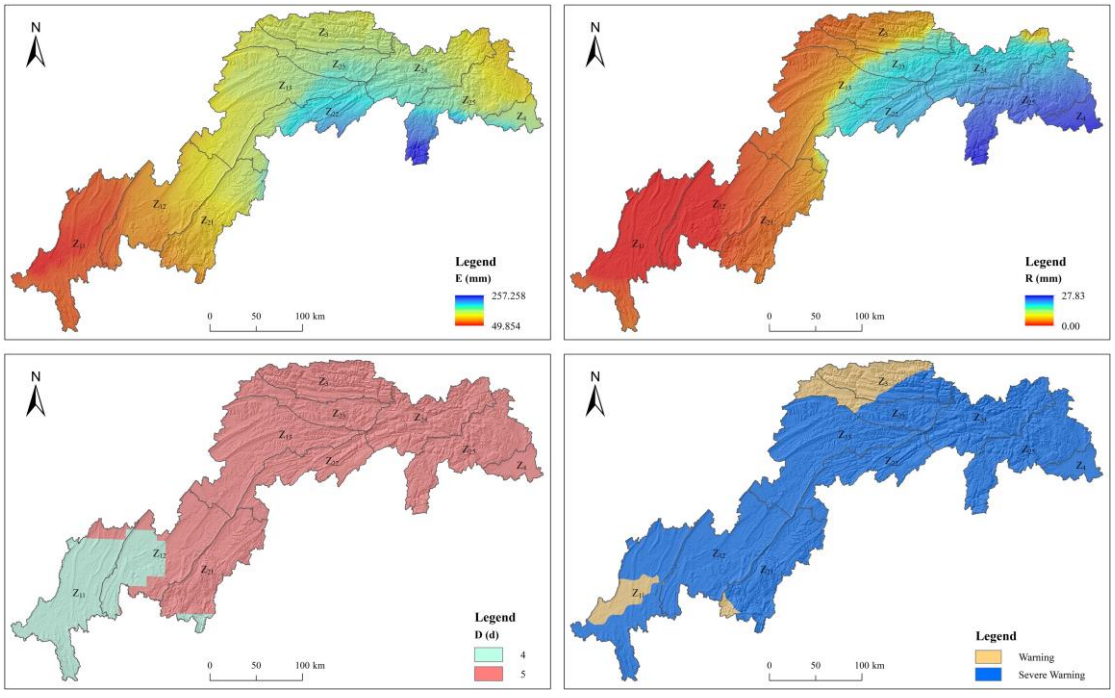

Figure 17: Various rainfall parameters and rainfall warning levels for 19 July 2020.

Based on the superposition matrix in Table 9, Fig. 17.d was superimposed on Figure 15 to obtain the LHW results for 19 July 2020 (Fig. 18).

https://doi.org/10.5194/nhess-2024-109
Preprint. Discussion started: 19 July 2024

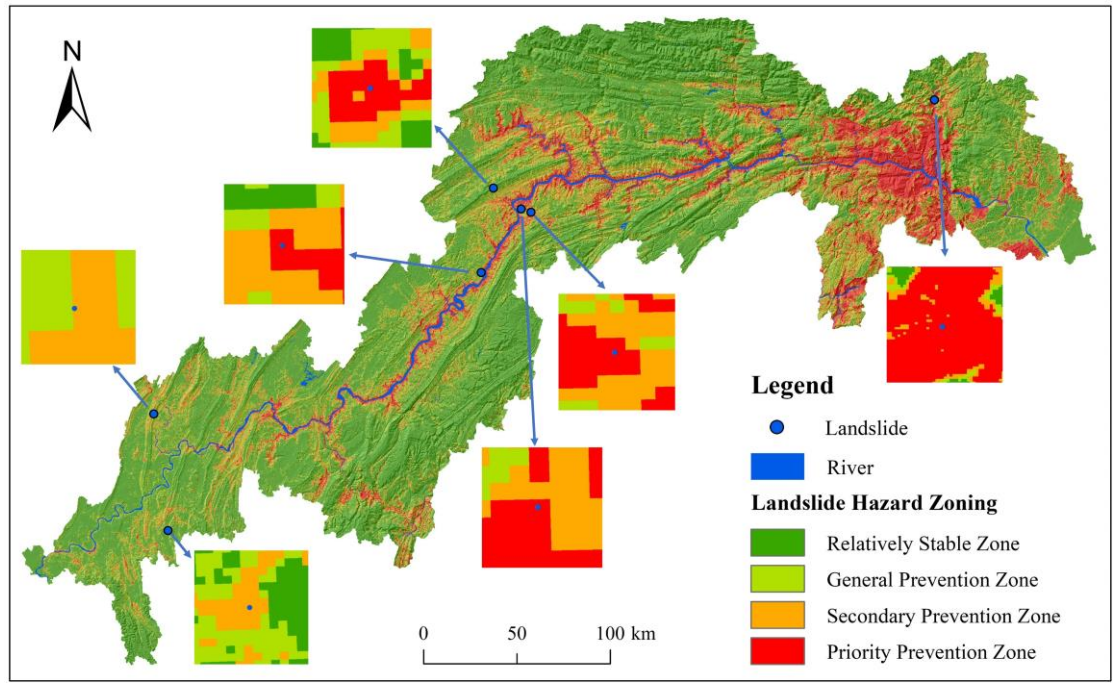

Figure 18: Landslide hazard warning results for 19 July 2020.

On July 19, 2020, there were seven landslide hazards, as shown in Fig. 18. Five of them fell in the priority prevention zone and two in the secondary prevention zone, demonstrating the accuracy of both the LHW results and the rainfall threshold model.

5. Discussion

5.1 Discussion of Rainfall Threshold Model

To investigate the best rainfall thresholds in the TGRA, two regression methods, OLS and MLP, and two RTM, E-D and E-D-R, are used in this study. Regardless of the regression approach, the results reveal that the E-D-R model has greater warning accuracy than the E-D model. In addition, the optimal RTM for two areas, Z_{13} and $Z_{23}Z_{24}Z_3$, are the E-D-R models obtained from the MLP regression, indicating the feasibility of using neural networks (MLP) for the study of RTM. However, since the dataset of this study is not large (only 453 landslides) nor complex (only 3 variables), it may not be able to clearly demonstrate the advantages of neural networks for rainfall threshold modeling. But we believe that this is a valuable attempt, and more variables such as peak rainfall and rainfall intensity can be added in subsequent studies, and the application of neural networks will certainly improve the accuracy of RWM.

https://doi.org/10.5194/nhess-2024-109
Preprint. Discussion started: 19 July 2024

Natural Hazards and Earth System Sciences
Discussions

To explore the reasons for the E-D-R model's higher warning accuracy, this study uses area Z_{12} as an example, and shows some of the points where the RWL has been changed (i.e. landslides where the RWL has been increased) in the R-E plane view (Fig. 19), where the colors of the landslides indicate the different RWL, and the meaning is the same as in Fig. 12.

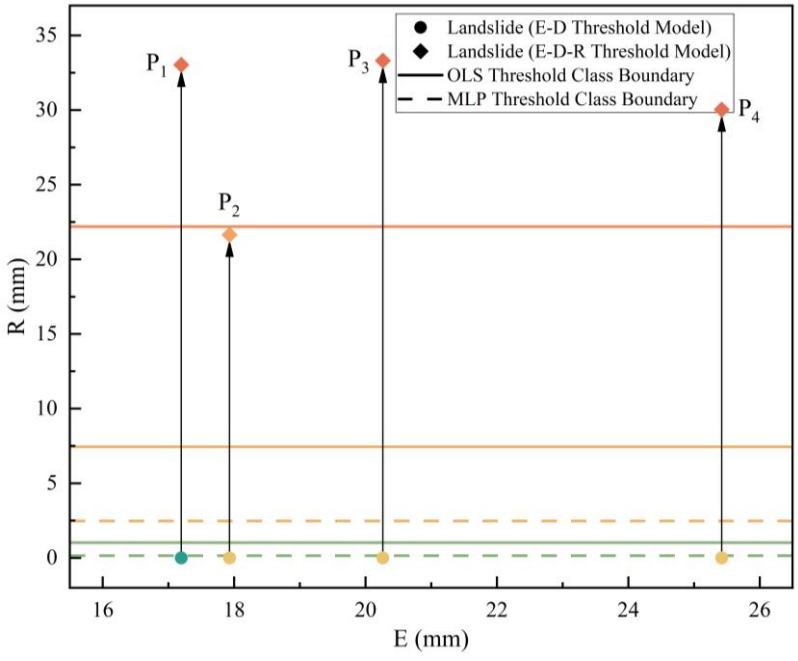

Figure 19: Rainfall warning level transition process (Z_{12} region).

The chart shows that after the R indication was added, the RWL of the four landslides rose dramatically. The warning level of P_1 in the E-D model was only "Caution", and the warning levels of the remaining three landslides were only "Special Caution", whereas in the E-D-R model using OLS regression, the warning level of P_2 was raised to "Warning", and the warning levels of the remaining three landslides were raised to "Severe Warning". Similarly, the alert levels of all four landslip points were raised to "Warning" in the E-D-R model using the MLP regression method. These landslides with RWL transition were the direct reason of the E-D-R model's improved accuracy in the Z_{12} region.

Further exploration of the rainfall process of these four landslides before the landslide occurred (Fig. 20) reveals that these four landslides received less rainfall in the four days before the landslide, resulting in a lower E, but more rainfall on the day of the landslide. The above characteristics make these four landslides have higher warning accuracy in the E-D-R RTM, indicating that the indicator R has some sensitivity in terms of landslides caused by heavy rain.

https://doi.org/10.5194/nhess-2024-109
Preprint. Discussion started: 19 July 2024

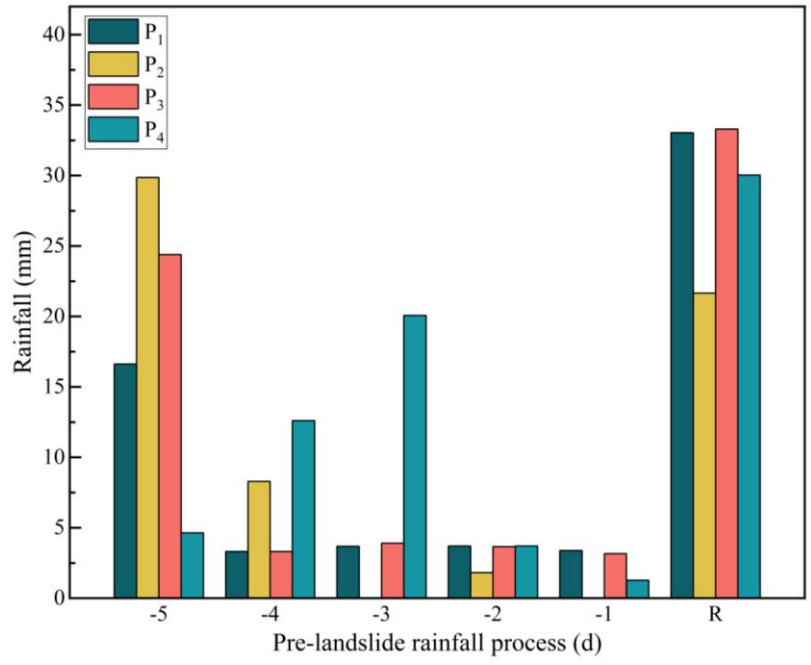

Figure 20: Rainfall processes at rainfall warning level transition points.

5.2 Discussion of Daily Landslide Hazard Warning

In this study, RF, SVM, and CNN-3D models were used to predict LS in the TGRA, and a comparison of the three models' results showed that the CNN-3D model predicts LS with more accuracy in the study area. In addition, further analysis of the CNN-3D model's LS results show that the very high LS zone is primarily distributed in areas with sparse vegetation, fragile stratigraphic lithology, close to rivers, and active human engineering activities, which is similar with the results of Wang et al (Wang et al., 2022a).

In terms of daily LHW, RWL are calculated using the optimal RTM for each sub-district based on forecast rainfall data from rainfall stations. Subsequently, the daily LHW results were derived by utilizing a superposition matrix to combine the RWL and LS results. On July 19, 2020, all seven landslide hazards are confirmed to be in the priority prevention and secondary prevention zones. It can be observed that the LHW results obtained through the RTM have very high accuracy and are of great significance in the prevention and control of landslide disasters. In addition, the process of transforming the LS results into LHW results through the RWL and superposition matrix is essentially a correction process of the LS results. After the correction, the areas that need to be focused on prevention and attention can be reduced to a certain extent, which saves the cost of manpower and material resources in landslide prevention and control.

https://doi.org/10.5194/nhess-2024-109
Preprint. Discussion started: 19 July 2024


Natural Hazards and Earth System Sciences Discussions

5.3 Practical Application of the Rainfall Threshold Model and Daily Landslide Hazard Warning

In the actual prevention and control of landslide hazards, it is inevitable to consider the factor of cost (Wang et al., 2023a). To safeguard as many people's lives and property as possible within the limited cost range, it is necessary to narrow and refine the regions that must be prioritized while guaranteeing the accuracy of the LHW results.

The E-D-R RTM, while considering the advantages of the E-D RTM, increases the sensitivity to landslides induced by heavy rainfall on the same day, and has higher landslide warning accuracy. Meanwhile, the CNN-3D model fully considers the spatial information around each raster point, and its predicted LS results have higher prediction accuracy than those of the RF and SVM models. Therefore, the E-D-R RTM and the CNN-3D model have a broad application space and development prospect in the warning and prevention of landslide disasters. The LHW results obtained by superposition of the results of the two models can ensure high accuracy and at the same time narrow down the areas that need to be focused on by virtue of the RWL results obtained by the RTM, so as to meet the requirements of landslide disaster prevention and control work.

In addition, although the E-D-R RTM as well as the CNN-3D model have high accuracy, there are certain uncertainties. For the RTM: (1) The rainfall station can only accurately reflect the rainfall situation of the site, and there will be inaccuracies and uncertainties whether the rainfall data are extended to the whole study area by interpolation or Thiessen polygon method. (2) Historical landslide data play a decisive influence on the results of the rainfall threshold model. Either less historical landslide data or the existence of more extreme rainfall conditions will lead to uncertainty in the final RWL. (3) Although this study divided 10 regions as well as both dry and rainy seasons for the rainfall threshold study, the overall regional scope is still large. There will be some uncertainty in the rainfall thresholds for different topography and geomorphology in the region. For the CNN-3D model, the selection of landslide-inducing factors, the size of the evaluation unit, the division ratio of the training set test set, and so on, will produce uncertainty in the results of LS.

Therefore, in the practical application of landslide prevention and control, it is necessary to combine the actual situation of the local area and select appropriate predisposing factors as well as evaluation units to ensure the accuracy of the LS results (Zhang et al., 2023). Simultaneously, a historical landslide database can be constructed. When a new landslide occurs, the corresponding rainfall data will be summarized into the database and the rainfall threshold of the area will be recalculated for the subsequent RWL. The uncertainty of the RTM is expected to reduce as the quantity of historical landslide data grows, and the rainfall thresholds will continue to converge to the ultimate rainfall thresholds for the region. Furthermore, when the historical landslide data are sufficiently rich, the region may be split further to constantly improve the accuracy of the rainfall warning level. Ultimately, the accuracy of LHW will be increased to give technical assistance for subsequent assessment of vulnerability as well as disaster preventive and mitigation efforts.

https://doi.org/10.5194/nhess-2024-109
Preprint. Discussion started: 19 July 2024


Natural Hazards and Earth System Sciences Discussions

6. Conclusion

Landslide disaster warning is an essential tool in the prevention and management of landslides. To improve the accuracy of landslide warning, this paper first chose two regression methods, MLP and OLS, and two RTM, E-D and E-D-R, and divided the TGRA into two dry and rainy seasons, as well as several sub-districts based on topography and rainfall, to explore the optimal RTM for the study area and obtain the daily RWL. Subsequently, 11 inducing factors were selected to investigate the LS in the study area utilizing three models: RF, SVM, and CNN-3D. Finally, using a superposition matrix, the RWL was overlaid on the LS results to achieve daily LHW in the TGRA.

In terms of rainfall threshold models, the study's results suggest that the E-D-R RTM has superior sensitivity in terms of landslides induced by heavy rainfall, therefore the rainfall warning accuracy produced by either regression method is higher than that of the E-D model. In addition, for each sub-district, the optimal RTM for the four zones Z_{11}, Z_{12}, $Z_{21}Z_{22}$, $Z_{25}Z_4$, and Dry Season is the E-D-R RTM calculated by OLS regression; whereas the optimal RTM for the two zones Z_{13} and $Z_{23}Z_{24}Z_3$ is the E-D-R RTM obtained by MLP regression. In terms of LS, the CNN-3D model's AUC and Accuracy achieved 0.96 and 0.9003, respectively, and its prediction accuracy outperformed the RF and SVM models.

The daily LHW is calculated by combining the daily RWL and the landslide susceptibility results. Data from the 19 July 2020 hazard event were utilized to verify the LHW results in this research. Of the seven landslide hazards on that date, five fell in the priority prevention zone and two in the secondary prevention zone, proving the accuracy of the LHW results and the RTM.

The RTM was utilized to obtain the daily RTL, and then overlaid with the LS results to obtain the daily LHW, which may be used as guidance and reference for local landslide disaster prevention and control operations. In addition, the introduction of MLP to regression analysis of rainfall threshold in this study also further enriches the calculation method of RTM, which is of some significance for promotion.

Code and data availability

The data and code can be accessed at https://doi.org/10.5281/zenodo.11311851 (Peng, 2024).

Author contributions

Bo Peng: Writing - original draft, Writing - review & editing, Data curation, Formal analysis, Validation.

Xueling Wu: Writing - review & editing, Funding acquisition, Conceptualization, Methodology.

https://doi.org/10.5194/nhess-2024-109
Preprint. Discussion started: 19 July 2024

Competing interests

The authors declare that they have no conflict of interest.

Disclaimer

Publisher's note: Copernicus Publications remains neutral with regard to jurisdictional claims made in the text, published maps, institutional affiliations, or any other geographical representation in this paper. While Copernicus Publications makes every effort to include appropriate place names, the final responsibility lies with the authors.

Acknowledgements

This study was supported by the National Natural Science Foundation of China (42071429).

Reference

Abraham, M. T., Pothuraju, D., and Satyam, N.: Rainfall Thresholds for Prediction of Landslides in Idukki, India: An Empirical Approach, Water, 11, 16, 2019.

Abraham, M. T., Satyam, N., Kushal, S., Rosi, A., Pradhan, B., and Segoni, S.: Rainfall Threshold Estimation and Landslide Forecasting for Kalimpong, India Using SIGMA Model, Water, 12, 13, 2020a.

Abraham, M. T., Satyam, N., Pradhan, B., and Alamri, A. M.: Forecasting of Landslides Using Rainfall Severity and Soil Wetness: A Probabilistic Approach for Darjeeling Himalayas, Water, 12, 19, 2020b.

Aksha, S. K., Resler, L. M., Juran, L., and Carstensen, L. W.: A geospatial analysis of multi-hazard risk in Dharan, Nepal, Geomat. Nat. Hazards Risk, 11, 88-111, 2020.

Baharvand, S., Rahnamarad, J., Soori, S., and Saadatkhah, N.: Landslide susceptibility zoning in a catchment of Zagros Mountains using fuzzy logic and GIS, Environ. Earth Sci., 79, 10, 2020.

Barcenas, O. U. E., Pioquinto, J. G. Q., Kurkina, E., and Lukyanov, O.: Surrogate Aerodynamic Wing Modeling Based on a Multilayer Perceptron, Aerospace, 10, 19, 2023.

Budimir, M. E. A., Atkinson, P. M., and Lewis, H. G.: A systematic review of landslide probability mapping using logistic regression, Landslides, 12, 419-436, 2015.

Cao, J. S., Qin, S. W., Yao, J. Y., Zhang, C. B., Liu, G. D., Zhao, Y. Y., and Zhang, R. C.: Debris flow susceptibility assessment based on information value and machine learning coupling method: from the perspective of sustainable development, Environ. Sci. Pollut. Res., doi: 10.1007/s11356-023-28575-w, 2023. 17, 2023.

Chan, H. C., Chen, P. A., and Lee, J. T.: Rainfall-Induced Landslide Susceptibility Using a Rainfall-Runoff Model and Logistic Regression, Water, 10, 18, 2018.

Chen, C. I. and Huang, S. J.: The necessary and sufficient condition for GM(1,1) grey prediction model, Appl. Math. Comput., 219, 6152-6162, 2013.

Chen, L. F., Guo, H. X., Gong, P. S., Yang, Y. Y., Zuo, Z. L., and Gu, M. Y.: Landslide susceptibility assessment using weights-of-evidence model and cluster analysis along the highways in the Hubei section of the Three Gorges Reservoir Area, Comput. Geosci., 156, 13, 2021.

Chen, T., Zhu, L., Niu, R. Q., Trinder, C. J., Peng, L., and Lei, T.: Mapping landslide susceptibility at the Three Gorges Reservoir, China, using gradient boosting decision tree, random forest and information value models, J Mt. Sci., 17, 670-685, 2020.

https://doi.org/10.5194/nhess-2024-109
Preprint. Discussion started: 19 July 2024

Chen, W., Peng, J. B., Hong, H. Y., Shahabi, H., Pradhan, B., Liu, J. Z., Zhu, A. X., Pei, X. J., and Duan, Z.: Landslide susceptibility modelling using GIS-based machine learning techniques for Chongren County, Jiangxi Province, China, Sci. Total Environ., 626, 1121-1135, 2018.

Chen, W. T., Li, X. J., Wang, Y. X., Chen, G., and Liu, S. W.: Forested landslide detection using LiDAR data and the random forest algorithm: A case study of the Three Gorges, China, Remote Sens. Environ., 152, 291-301, 2014.

Cheng, J. Y., Dai, X. A., Wang, Z. K., Li, J. Z., Qu, G., Li, W. L., She, J. X., and Wang, Y. L.: Landslide Susceptibility Assessment Model Construction Using Typical Machine Learning for the Three Gorges Reservoir Area in China, Remote Sens., 14, 28, 2022.

Chung, M. C., Tan, C. H., and Chen, C. H.: Local rainfall thresholds for forecasting landslide occurrence: Taipingshan landslide triggered by Typhoon Saola, Landslides, 14, 19-33, 2017.

Ciurleo, M., Mandaglio, M. C., and Moraci, N.: Landslide susceptibility assessment by TRIGRS in a frequently affected shallow instability area, Landslides, 16, 175-188, 2019.

Cobos-Mora, S. L., Rodriguez-Galiano, V., and Lima, A.: Analysis of landslide explicative factors and susceptibility mapping in an andean context: The case of Azuay province (Ecuador), Heliyon, 9, 17, 2023.

Dahal, R. K. and Hasegawa, S.: Representative rainfall thresholds for landslides in the Nepal Himalaya, Geomorphology, 100, 429-443, 2008.

Fan, X. L., Feng, X. F., Dong, Y. Y., and Hou, H. C.: COVID-19 CT image recognition algorithm based on transformer and CNN, Displays, 72, 9, 2022.

Gariano, S. L., Supplizi, G. V., Ardizzone, F., Salvati, P., Bianchi, C., Morbidelli, R., and Saltalippi, C.: Long-term analysis of rainfall-induced landslides in Umbria, central Italy, Nat. Hazards, 106, 2207-2225, 2021.

Gill, H. S., Khalaf, O. I., Alotaibi, Y., Alghamdi, S., and Alassery, F.: Multi-Model CNN-RNN-LSTM Based Fruit Recognition and Classification, Intell. Autom. Soft Comput., 33, 637-650, 2022.

Guo, B., Pei, X. J., Xu, M., and Li, T. T.: Analyzing Rainfall Threshold for Shallow Landslides Using Physically Based Modeling in Rasuwa District, Nepal, Water, 14, 12, 2022.

Guo, Z. Z., Shi, Y., Huang, F. M., Fan, X. M., and Huang, J. S.: Landslide susceptibility zonation method based on C5.0 decision tree and K-means cluster algorithms to improve the efficiency of risk management, Geosci. Front., 12, 19, 2021.

Habumugisha, J. M., Chen, N. S., Rahman, M., Islam, M. M., Ahmad, H., Elbeltagi, A., Sharma, G., Liza, S. N., and Dewan, A.: Landslide Susceptibility Mapping with Deep Learning Algorithms, Sustainability, 14, 22, 2022.

Hasan, M. M., Nilay, M. S. M., Jibon, N. H., and Rahman, R. M.: LULC changes to riverine flooding: A case study on the Jamuna River, Bangladesh using the multilayer perceptron model, Results Eng., 18, 19, 2023.

He, Q. F., Shahabi, H., Shirzadi, A., Li, S. J., Chen, W., Wang, N. Q., Chai, H. C., Bian, H. Y., Ma, J. Q., Chen, Y. T., Wang, X. J., Chapi, K., and Bin Ahmad, B.: Landslide spatial modelling using novel bivariate statistical based Naive Bayes, RBF Classifier, and RBF Network machine learning algorithms, Sci. Total Environ., 663, 1-15, 2019.

He, S. S., Wang, J., and Liu, S. N.: Rainfall Event-Duration Thresholds for Landslide Occurrences in China, Water, 12, 17, 2020.

Hoffman, S. and Jasinski, R.: The Use of Multilayer Perceptrons to Model PM2.5 Concentrations at Air Monitoring Stations in Poland, Atmosphere, 14, 19, 2023.

Huang, F. M., Cao, Z. S., Jiang, S. H., Zhou, C. B., Huang, J. S., and Guo, Z. Z.: Landslide susceptibility prediction based on a semi-supervised multiple-layer perceptron model, Landslides, 17, 2919-2930, 2020.

Huang, F. M., Chen, J. W., Liu, W. P., Huang, J. S., Hong, H. Y., and Chen, W.: Regional rainfall-induced landslide hazard warning based on landslide susceptibility mapping and a critical rainfall threshold, Geomorphology, 408, 16, 2022a.

Huang, F. M., Yan, J., Fan, X. M., Yao, C., Huang, J. S., Chen, W., and Hong, H. Y.: Uncertainty pattern in landslide susceptibility prediction modelling: Effects of different landslide boundaries and spatial shape expressions, Geosci. Front., 13, 16, 2022b.

Jiang, P., Zeng, Z. G., Chen, J. J., Tang, H. M., and Ieee: A PSOGSA method to optimize the T-S fuzzy neural network for displacement prediction of landslide, San Diego, CA, Oct 05-08 2014, 1216-1221, 2014.

https://doi.org/10.5194/nhess-2024-109
Preprint. Discussion started: 19 July 2024

Jin, L., Li, Z. C., and Tang, J. H.: Deep Semantic Multimodal Hashing Network for Scalable Image-Text and Video-Text Retrievals, IEEE Trans. Neural Netw. Learn. Syst., 34, 1838-1851, 2023.

Kaliyar, R. K., Goswami, A., and Narang, P.: FakeBERT: Fake news detection in social media with a BERT-based deep learning approach, Multimed. Tools Appl., 80, 11765-11788, 2021.

Kumar, P. C. M. and Kavitha, R.: Prediction of nanofluid viscosity using multilayer perceptron and Gaussian process regression, J. Therm. Anal. Calorim., 144, 1151-1160, 2021.

Lee, M. L., Ng, K. Y., Huang, Y. F., and Li, W. C.: Rainfall-induced landslides in Hulu Kelang area, Malaysia, Nat. Hazards, 70, 353-375, 2014.

Li, W. J., Fang, Z. C., and Wang, Y.: Stacking ensemble of deep learning methods for landslide susceptibility mapping in the Three Gorges Reservoir area, China, Stoch. Environ. Res. Risk Assess., 36, 2207-2228, 2022.

Lim, D. H., Na, W. J., Hong, W. H., and Bae, Y. H.: Development of a fire prediction model at the urban planning stage: Ordinary least squares regression analysis of the area of urban land use and fire damage data in South Korea, Fire Saf. J., 136, 8, 2023.

Liu, M. M., Liu, J. P., Xu, S. H., Chen, C., Bao, S., Wang, Z. L., and Du, J.: 3DCNN landslide susceptibility considering spatial-factor features, Front. Environ. Sci., 11, 12, 2023.

Liu, X., Yin, K., Xiao, C., Chen, L., Zeng, T., Li, Y., Liu, Z., Gong, Q., and Chen, W.: Meteorological early warning of landslide based on I-D-R threshold model, Earth Science, 2022. 1-15. (in Chinese), 2022.

Long, J. J., Liu, Y., Li, C. D., Fu, Z. Y., and Zhang, H. K.: A novel model for regional susceptibility mapping of rainfall-reservoir induced landslides in Jurassic slide-prone strata of western Hubei Province, Three Gorges Reservoir area, Stoch. Environ. Res. Risk Assess., 35, 1403-1426, 2021.

Marin, R. J.: Physically based and distributed rainfall intensity and duration thresholds for shallow landslides, Landslides, 17, 2907-2917, 2020.

Marin, R. J., Garcia, E. F., and Aristizabal, E.: Effect of basin morphometric parameters on physically-based rainfall thresholds for shallow landslides, Eng. Geol., 278, 16, 2020.

Martinovic, K., Gavin, K., Reale, C., and Mangan, C.: Rainfall thresholds as a landslide indicator for engineered slopes on the Irish Rail network, Geomorphology, 306, 40-50, 2018.

Mathew, J., Babu, D. G., Kundu, S., Kumar, K. V., and Pant, C. C.: Integrating intensity-duration-based rainfall threshold and antecedent rainfall-based probability estimate towards generating early warning for rainfall-induced landslides in parts of the Garhwal Himalaya, India, Landslides, 11, 575-588, 2014.

Mei, J. Q., Chen, W. Y., Li, B. Y., Li, S. X., Zhang, J., and Yan, J.: Adaptive fusion of multi-exposure images based on perceptron model, Appl. Math. Nonlinear Sci., doi: 10.2478/amns.2023.1.00053, 2023. 14, 2023.

Narimani, R., Jun, C. H. Y., De Michele, C., Gan, T. Y., Nezhad, S. M., and Byun, J.: Multilayer perceptron-based predictive model using wavelet transform for the reconstruction of missing rainfall data, Stoch. Environ. Res. Risk Assess., 37, 2791-2802, 2023.

Niu, R. Q., Wu, X. L., Yao, D. K., Peng, L., Ai, L., and Peng, J. H.: Susceptibility Assessment of Landslides Triggered by the Lushan Earthquake, April 20, 2013, China, IEEE J. Sel. Top. Appl. Earth Observ. Remote Sens., 7, 3979-3992, 2014.

Peng, B.: Rainfall threshold data for landslides in the Three Gorges reservoir area [Data set]. Zenodo. https://doi.org/10.5281/zenodo.11311851, 2024.

Peruccacci, S., Brunetti, M. T., Gariano, S. L., Melillo, M., Rossi, M., and Guzzetti, F.: Rainfall thresholds for possible landslide occurrence in Italy, Geomorphology, 290, 39-57, 2017.

Pradhan, A. M. S., Kang, H. S., Lee, J. S., and Kim, Y. T.: An ensemble landslide hazard model incorporating rainfall threshold for Mt. Umyeon, South Korea, Bull. Eng. Geol. Environ., 78, 131-146, 2019.

Rohan, T., Shelef, E., Mirus, B., and Coleman, T.: Prolonged influence of urbanization on landslide susceptibility, Landslides, 20, 1433-1447, 2023.

Rossi, M., Luciani, S., Valigi, D., Kirschbaum, D., Brunetti, M. T., Peruccacci, S., and Guzzetti, F.: Statistical approaches for the definition of landslide rainfall thresholds and their uncertainty using rain gauge and satellite data, Geomorphology, 285, 16-27, 2017.

https://doi.org/10.5194/nhess-2024-109
Preprint. Discussion started: 19 July 2024

Salee, R., Chinkulkijniwat, A., Yubonchit, S., Horpibulsuk, S., Wangfaoklang, C., and Soisompong, S.: New threshold for landslide warning in the southern part of Thailand integrates cumulative rainfall with event rainfall depth-duration, Nat. Hazards, 113, 125-141, 2022.

Sarkar, S., Chandna, P., Pandit, K., and Dahiya, N.: An event-duration based rainfall threshold model for landslide prediction in Uttarkashi region, North-West Himalayas, India, Int. J. Earth Sci., doi: 10.1007/s00531-023-02337-y, 2023. 17, 2023.

Segoni, S., Tofani, V., Rosi, A., Catani, F., and Casagli, N.: Combination of Rainfall Thresholds and Susceptibility Maps for Dynamic Landslide Hazard Assessment at Regional Scale, Front. Earth Sci., 6, 11, 2018.

Selamat, S. N., Abd Majid, N., Taha, M. R., and Osman, A.: Landslide Susceptibility Model Using Artificial Neural Network (ANN) Approach in Langat River Basin, Selangor, Malaysia, Land, 11, 21, 2022.

Sheng, Y. F., Li, Y. Y., Xu, G. L., and Li, Z. G.: Threshold assessment of rainfall-induced landslides in Sangzhi County: statistical analysis and physical model, Bull. Eng. Geol. Environ., 81, 15, 2022.

Soralump, S., Shrestha, A., Thowiwat, W., Sukjaroen, R., Chaithong, T., Yangsanphu, S., Koirala, A., and Jotisankasa, A.: Assessment of landslide behaviour in colluvium deposit at Doi Chang, Thailand, Sci Rep, 11, 12, 2021.

Teja, T. S., Dikshit, A., and Satyam, N.: Determination of Rainfall Thresholds for Landslide Prediction Using an Algorithm-Based Approach: Case Study in the Darjeeling Himalayas, India, Geosciences, 9, 9, 2019.

Wang, C., Wang, X. D., Zhang, H. Y., Meng, F. Q., and Li, X. L.: Assessment of environmental geological disaster susceptibility under a multimodel comparison to aid in the sustainable development of the regional economy, Environ. Sci. Pollut. Res., 30, 6573-6591, 2023a.

Wang, X. B., Zhao, Y. Q., and Li, W. F.: Recognition of Commercial Vehicle Driving Cycles Based on Multilayer Perceptron Model, Sustainability, 15, 21, 2023b.

Wang, X. L., Zhang, L. Q., Wang, S. J., and Lari, S.: Regional landslide susceptibility zoning with considering the aggregation of landslide points and the weights of factors, Landslides, 11, 399-409, 2014.

Wang, X. N., Zhang, X. L., Bi, J., Zhang, X. D., Deng, S. Q., Liu, Z. W., Wang, L. Z., and Guo, H. X.: Landslide Susceptibility Evaluation Based on Potential Disaster Identification and Ensemble Learning, Int. J. Environ. Res. Public Health, 19, 26, 2022a.

Wang, Z. Y., Ma, C. M., Qiu, Y., Xiong, H. X., and Li, M. H.: Refined Zoning of Landslide Susceptibility: A Case Study in Enshi County, Hubei, China, Int. J. Environ. Res. Public Health, 19, 22, 2022b.

Wu, C. Y. and Yeh, Y. C.: A Landslide Probability Model Based on a Long-Term Landslide Inventory and Rainfall Factors, Water, 12, 17, 2020.

Wu, Y. M., Lan, H. X., Gao, X., Li, L. P., and Yang, Z. H.: A simplified physically based coupled rainfall threshold model for triggering landslides, Eng. Geol., 195, 63-69, 2015.

Xia, P., Hu, X. L., Wu, S. S., Ying, C. Y., and Liu, C.: Slope Stability Analysis Based on Group Decision Theory and Fuzzy Comprehensive Evaluation, J. Earth Sci., 31, 1121-1132, 2020.

Xing, X. F., Wu, C. L., Li, J. H., Li, X. Y., Zhang, L. M., and He, R. J.: Susceptibility assessment for rainfall-induced landslides using a revised logistic regression method, Nat. Hazards, 106, 97-117, 2021.

Yang, H. J., Wei, F. Q., Ma, Z. F., Guo, H. Y., Su, P. C., and Zhang, S. J.: Rainfall threshold for landslide activity in Dazhou, southwest China, Landslides, 17, 61-77, 2020.

Yang, Z. Q., Xu, C., Shao, X. Y., Ma, S. Y., and Li, L.: Landslide susceptibility mapping based on CNN-3D algorithm with attention module embedded, Bull. Eng. Geol. Environ., 81, 21, 2022.

Youssef, A. M., Pradhan, B., Dikshit, A., Al-Katheri, M. M., Matar, S. S., and Mahdi, A. M.: Landslide susceptibility mapping using CNN-1D and 2D deep learning algorithms: comparison of their performance at Asir Region, KSA, Bull. Eng. Geol. Environ., 81, 22, 2022.

Yu, L. B., Zhou, C., Wang, Y., Cao, Y., and Peres, D. J.: Coupling Data- and Knowledge-Driven Methods for Landslide Susceptibility Mapping in Human-Modified Environments: A Case Study from Wanzhou County, Three Gorges Reservoir Area, China, Remote Sens., 14, 21, 2022.

Yuniawan, R. A., Rifa'i, A., Faris, F., Subiyantoro, A., Satyaningsih, R., Hidayah, A. N., Hidayat, R., Mushthofa, A., Ridwan, B. W., Priangga, E., Muntohar, A. S., Jetten, V. G., van Westen, C. J., den Bout, B. V., and Sutanto, S. J.:

https://doi.org/10.5194/nhess-2024-109
Preprint. Discussion started: 19 July 2024

Revised Rainfall Threshold in the Indonesian Landslide Early Warning System, Geosciences, 12, 17, 2022.
Zhang, H., Yin, C., Wang, S. P., and Guo, B.: Landslide susceptibility mapping based on landslide classification and
630 improved convolutional neural networks, Nat. Hazards, doi: 10.1007/s11069-022-05748-3, 2022. 41, 2022.
Zhang, J. Y., Ma, X. L., Zhang, J. L., Sun, D. L., Zhou, X. Z., Mi, C. L., and Wen, H. J.: Insights into geospatial heterogeneity of landslide susceptibility based on the SHAP-XGBoost model, J. Environ. Manage., 332, 20, 2023.
Zhao, B. R., Dai, Q., Han, D. W., Dai, H. C., Mao, J. Q., and Zhuo, L.: Probabilistic thresholds for landslides warning by integrating soil moisture conditions with rainfall thresholds, J. Hydrol., 574, 276-287, 2019.
635 Zhao, L. H., Liu, M., Song, Z. C., Wang, S. G., Zhao, Z. G., and Zuo, S.: Regional-scale modeling of rainfall-induced landslides under random rainfall patterns, Environ. Modell. Softw., 155, 14, 2022.
Zhou, C., Cao, Y., Hu, X., Yin, K. L., Wang, Y., and Catani, F.: Enhanced dynamic landslide hazard mapping using MT-InSAR method in the Three Gorges Reservoir Area, Landslides, 19, 1585-1597, 2022.
Zhu, C. H. and Hu, G. D.: Time Series Prediction of Landslide Displacement Using SVM Model: Application to
640 Baishuihe Landslide in Three Gorges Reservoir Area, China, Guangzhou, PEOPLES R CHINA, Sep 15-16 2012, 1413-+, 2013.